



Review

Some Theoretical Aspects of Tertiary Treatment of Water/Oil Emulsions by Adsorption and Coalescence Mechanisms: A Review

Patrik Sobolčiak¹, Anton Popelka¹, Aisha Tanvir¹, Mariam A. Al-Maadeed² , Samer Adham³  and Igor Krupa^{1,*}

¹ Center for Advanced Materials, Qatar University, P.O. Box 2713 Doha, Qatar; patrik@qu.edu.qa (P.S.); anton.popelka@qu.edu.qa (A.P.); aisha.tanvir1991@gmail.com (A.T.)

² Materials Science & Technology Program (MATS), College of Arts & Sciences, Qatar University, P.O. Box 2713 Doha, Qatar; m.alali@qu.edu.qa

³ GWSC-ConocoPhillips, Qatar Science & Technology Park, Tech 2 Building, No.109, P.O. Box 24750 Doha, Qatar; Samer.Adham@conocophillips.com

* Correspondence: igor.krupa@qu.edu.qa



Citation: Sobolčiak, P.; Popelka, A.; Tanvir, A.; Al-Maadeed, M.A.; Adham, S.; Krupa, I. Some Theoretical Aspects of Tertiary Treatment of Water/Oil Emulsions by Adsorption and Coalescence Mechanisms: A Review. *Water* **2021**, *13*, 652. <https://doi.org/10.3390/w13050652>

Academic Editor: Cidália Botelho

Received: 2 January 2021

Accepted: 15 February 2021

Published: 28 February 2021

Publisher's Note: MDPI stays neutral with regard to jurisdictional claims in published maps and institutional affiliations.



Copyright: © 2021 by the authors. Licensee MDPI, Basel, Switzerland. This article is an open access article distributed under the terms and conditions of the Creative Commons Attribution (CC BY) license (<https://creativecommons.org/licenses/by/4.0/>).

Abstract: The massive increase in the volumes of oily contaminated produced waters associated with various industrial sectors has initiated considerable technological and scientific efforts related to the development of new cleaning strategies. The petrochemical industry (oil and gas production and processing) contributes to those volumes by approximately 340 billion barrels per year. The removal of emulsified oily components is a matter of particular interest because the high emulsion stability necessitates sophisticated technological approaches as well as a deep theoretical understanding of key mechanisms of oil/water separation. This review deals with the theoretical aspects of the treatment of emulsified oil/water mixtures and is particularly focused on tertiary treatment, which means the reduction of the oil content from 70–100 ppm to below 10 ppm, depending on national regulations for water discharge. The review concerns the mechanisms of oil/water separation and it covers the (i) adsorption isotherms, (ii) kinetics of adsorption, (iii) interfacial interactions between oil/water mixtures and solid surfaces, and (iv) oil/water separation techniques based on the wettability of solid/oil/water interfaces. The advantages and drawbacks of commonly used as well as newly proposed kinetic and adsorption models are reviewed, and their applicability for the characterization of oil/water separation is discussed. The lack of suitable adsorption isotherms that can be correctly applied for a description of oil adsorption at external and internal solid surfaces of both nonporous and porous structures is pointed out. The direct using of common isotherms, which were originally developed for gas adsorption, often leads to the incorrect data description because the adsorption of oily components at solid surfaces does not fit the assumptions from which these models were originally derived. Particularly, it results in problematic calculations of the thermodynamic parameters of sorption. The importance of nonlinear analysis of data is discussed, since recent studies have indicated that the error structure of experimental data is usually changed if the original nonlinear adsorption isotherms are transformed into their linearized forms. The comparison between the pseudo-first-order and pseudo-second-order kinetic models was performed. It was shown that the correlation between data and models strongly depends on the selection of data, particularly on the frequency of collected data in time scale. The wettability of solid surfaces by oil in air and under water is discussed, regarding the surface morphology of surfaces. We demonstrate that the combination of surface chemistry and topology strongly influences the separation of oil/water emulsions.

Keywords: produced water; tertiary treatment; deep-bed media; adsorption; kinetic models; wettability

1. Introduction

Oil and grease (O&G) are organic substances composed of hydrocarbons, fatty acids, soaps (surfactants), lipids and waxes. Petroleum wastewaters from various sources (crude

oil, gas, shale gas extraction and oil refineries) represent the largest volumes of oily polluted waters, followed by metal processing wastewater and food processing wastewater [1]. As an illustration, the global volumes of produced water volumes were 202 billion barrels in 2014 and were estimated to be approximately 340 billion barrels in 2020 [2]. The estimated produced water volume from shale reservoirs over the first 5–10 years of production ranges from 1.7 to 14.3 million liters per well [3]. Emulsification of oil/water mixtures is a phenomenon frequently occurring in water treatment processes because emulsifiers and surfactants alter the chemical character of an oil droplet surface. In the petroleum industry, chemically enhanced oil recovery (EOR) leads to the production of a vast amount of oil-emulsified wastewater because surfactants (together with polymers such as polyacrylamide and alkaline compounds) are key additives that are flooded into wells in order to enhance the recovery of bypass oil and oil trapped in porous reservoirs [4]. Both anionic and cationic surfactants are used, dependent on the character of natural reservoirs of oil and gas [5]. More details about various aspects of EOR and applied surfactants can be found in the review of Gbadamosi et al. [6]. The promotion of emulsion instabilities is an important feature that contributes to the separation process in deep-bed filtration. The most important phenomenon in the destabilization of oil-in-water emulsions is coalescence. More details about the mechanisms of coalescence, experimental techniques, and modeling can be found, for instance, in the review of Kamp et al. [7], and the theoretical aspects of emulsions' stability are described in the chapter by Danov [8]. On the other hand, conservation of a long-term stability of emulsions is a crucial point in the food and cosmetic industry. Various types of surfactants (such as small molecule surfactants, phospholipids, proteins, and polysaccharides [9]) and their mixtures have been studied recently, as summarized in review of McClements et al. [10], gelatin-based emulsifiers were summarized by Ting Zang et al. [11], and water-in-oil emulsions stabilized by surfactants, biopolymers and particles were reviewed by Zembyla et al. [12].

In the petroleum industry, chemically enhanced oil recovery leads to the production of a vast amount of oil-emulsified wastewater. The key factors that influence the efficiency of emulsion separation are the properties of the filtration medium, namely, the (i) surface free energy, (ii) roughness and pore size, (iii) size, and (iv) permeability; the properties of the dispersed and continuous phase, namely, the (i) droplet size, (ii) interfacial tension, (iii) densities of components, (iv) viscosity, and (v) presence of surfactants; and the operating conditions, namely, the (i) inflow velocity, (ii) pressure drop, (iii) emulsion concentration, (iv) temperature, and (v) filter and flow orientation [13].

Deep-bed filtration involves three fundamental mechanisms: (i) transport mechanism, (ii) attachment mechanism, and (iii) detachment mechanism. The transport mechanism includes straining, interception, inertia, sedimentation, diffusion, and hydrodynamic action [14]. The attachment mechanism is realized by London–Van der Waals forces, Born repulsive forces, hydration, mutual adsorption, hydrophobic effects, and steric interactions [15]. The detachment mechanism involves reverse flow flushing and coalescence. The transport mechanism is not discussed in this review, and much relevant information can be found in the comprehensive review of Jegatheesan and Vigneswaran [15]. In this review, the main attention is given to the attachment and detachment mechanisms, including adsorption isotherms, kinetic models, diffusion in adsorbents, wettability of surfaces, and induced coalescence on solid surfaces.

2. Adsorption Isotherms

The most important factors affecting the adsorption process are listed in Figure 1.

Adsorbents occur in various forms such as powder, small pellets, beads or granules, with a very porous structure having fine pores and pore volumes up to 50% of total particle volume. The most important feature of an adsorbent is the porous structure resulting in high surface area; a highly porous solid may be carbonaceous or inorganic in nature, synthetic or naturally occurring, and in certain circumstances may have true molecular sieving properties. Many adsorbent materials are amorphous and contain

complex networks of interconnected micropores ($D < 2$ nm), mesopores ($2 \text{ nm} < D < 50$ nm) and macropores ($D > 50$ nm). Adsorbing molecules must first pass through the fluid film, which is external to the adsorbent particle, then through the macroporous structure into the micropores where the molecules are adsorbed. Figure 2 illustrates the different types of pores.

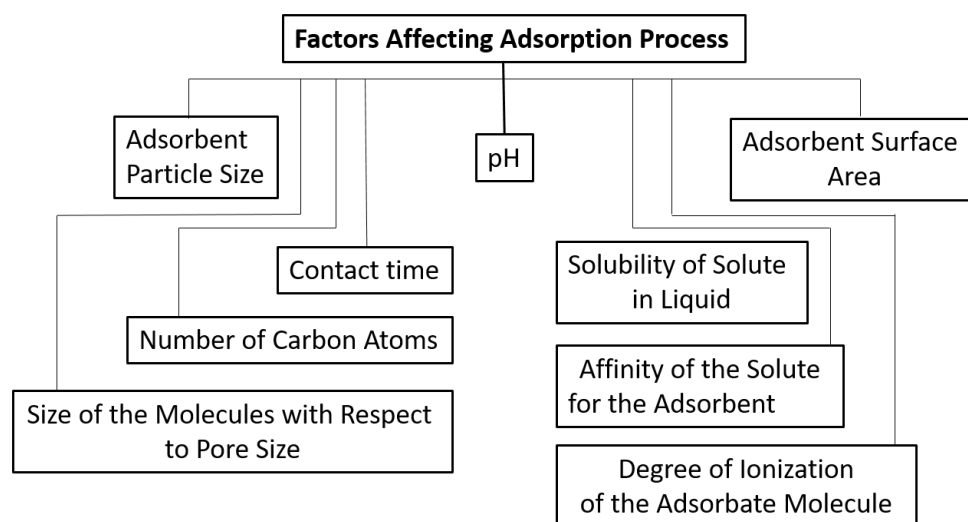


Figure 1. The most important factors affecting the adsorption process (adapted from: Muftah H. El-Naas [16]).

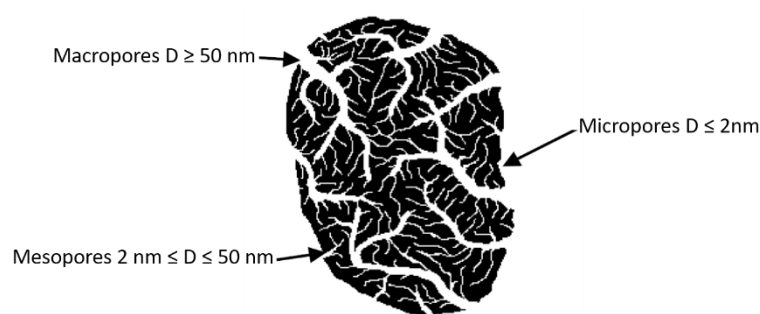


Figure 2. Schematic representation of the different types of pores. (adapted from: Muftah H. El-Naas [16]).

Porosity strongly depends on the processing conditions. For instance, polyethylene pellets, which always have smooth surfaces as a consequence of the route of preparation (extrusion) (Figure 3A) and linear density polyethylene (LDPE) powders, depending on the route of the preparation (mostly grinding; partly precipitation from a solution) can have very porous structures, as demonstrated by SEM and profilometry analysis and shown in Figure 3A–C. It results in an increase of the specific surface area in 32,300% at the same average dimensions.

The physical models, which describe the dependence of the amount of adsorbed species on the equilibrium concentration of those species in bulk solution at constant temperature, are called adsorption isotherms. The majority of common adsorption isotherms were originally developed for gas adsorption and then adapted for the adsorption of liquids or species dissolved or dispersed in liquids. There are some features that differentiate the applicability of adsorption isotherms for liquids in comparison to gases [17], as will be discussed below.

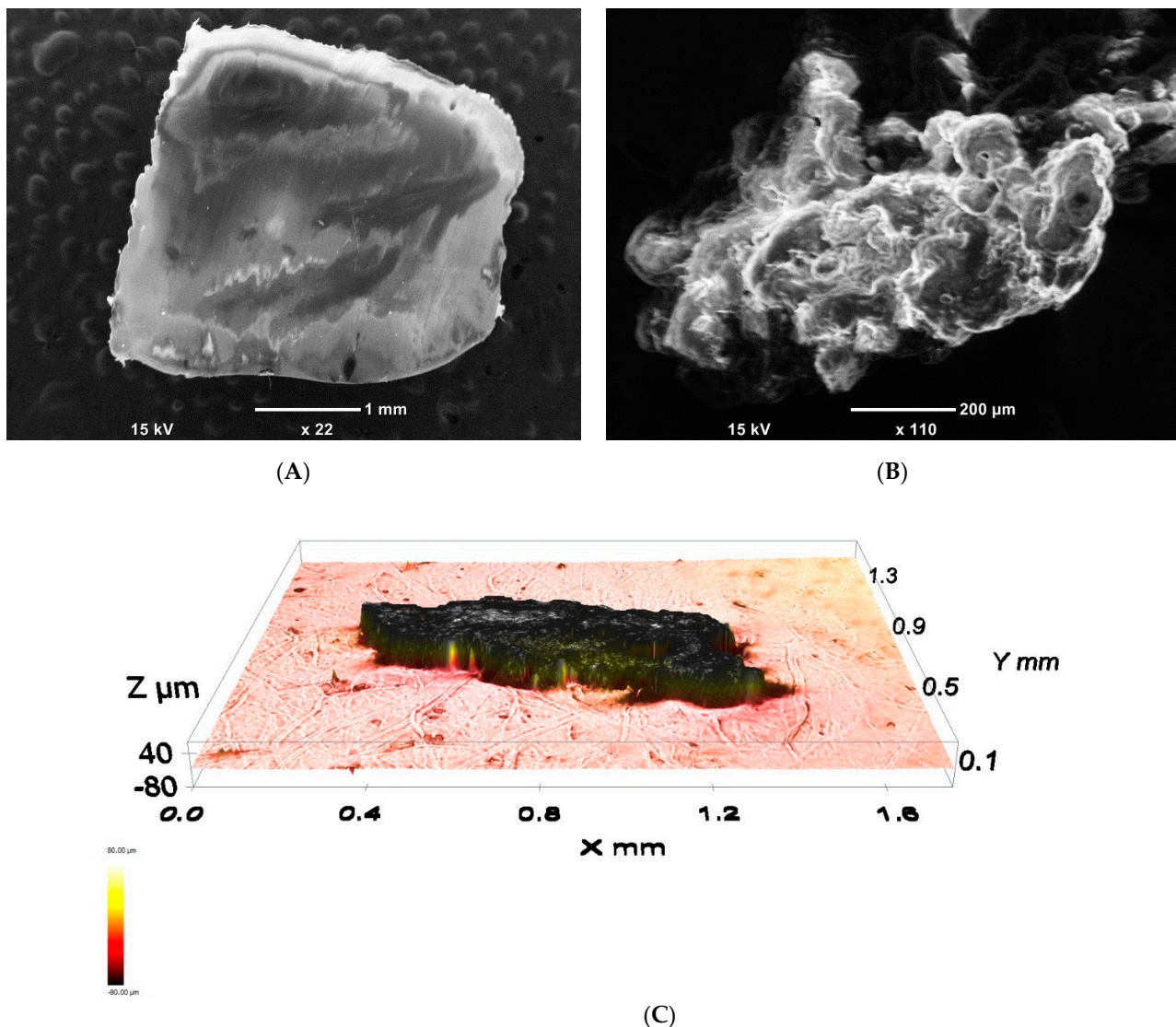


Figure 3. SEM micrograph of a common as-produced LDPE pellet (A), SEM micrograph (B) and profilometry image (C) of LDPE powder prepared by grinding (unpublished results).

2.1. Langmuir Isotherm (LI)

The LI is the most commonly mentioned isotherm in the literature for both gases and liquids [18–22]; however, adsorption from liquids does not frequently fit the assumptions used for LI derivation. These assumptions are that (a) adsorbed species can form only a monolayer and that (b) all the reaction sites on the surface of the adsorbent are equivalent. This implies that the enthalpy of adsorption is independent of the surface coverage, that (c) a molecule (individual species) can be adsorbed on at a vacant site, and that (d) the probability of adsorption is independent of the occupation of neighboring sites (no interaction between adsorbed species). The LI is expressed in the form given by Equation (1) or in its linear form.

$$q_e = \frac{K_L q_m c_e}{1 + K_L c_e} \quad (1)$$

where c_e (mg/L) is the equilibrium concentration, q_e (mg/g) is the equilibrium adsorption capacity of the adsorbent, q_m (mg/g) is the maximum adsorption capacity, and $K_L = k_a/k_d$ is the Langmuir adsorption (equilibrium) constant.

The LI is often expressed in linear form (Equation (2)), which simplifies the determination of unknown parameters (q_m , K_L) using linear regression. The boundaries of linearity are also the boundaries of validity of the LI.

$$\frac{c_e}{q_e} = \frac{1}{K_L q_m} + \frac{c_e}{q_m} \quad (2)$$

A useful parameter associated with the LI is called the separation factor R_L (Equation (3)).

$$R_L = \frac{1}{1 + K_L c_0} \quad (3)$$

R_L corresponds to the adsorption processes according to the following criteria [23]:

Case I. $R_L > 1$: The adsorption is unfavorable (an increase in Gibbs free energy of adsorption).

Case II. $1 > R_L > 0$: The adsorption is favorable (a decrease in Gibbs free energy).

Case III. $R_L = 1$: It characterizes a linear adsorption (unoccupied sites at the adsorbent are randomly occupied by adsorbate proportionally to their concentration, and only one reaction site is occupied by one species).

Case IV. $R_L = 0$: The desorption process is irreversible.

The key disadvantage of the LI is that it fails to describe adsorption at rough surfaces of the adsorbent. Rough inhomogeneous surfaces have multiple site types available for adsorption, and some parameters, such as the heat of adsorption, vary from site to site.

2.2. Brunauer–Emmet–Teller (BET) Isotherm

The BET isotherm, expressed by Equation (4), is the most widely employed isotherm for describing the multilayer adsorption of gases, and it has been adapted for the adsorption of/from liquids [24–26]. There is no limit on how many layers can be deposited on the surface.

$$\frac{q_e}{q_m} = \frac{C \frac{c_e}{c_s}}{\left(1 - \frac{c_e}{c_s}\right) \left(1 - \left(\frac{c_e}{c_s} + C \frac{c_e}{c_s}\right)\right)} \quad (4)$$

where c_e (mg/L) is an equilibrium concentration, q_e (mg/g) is the equilibrium adsorption capacity of the adsorbent, q_m (mg/g) is the maximum adsorption capacity, c_s is the saturation concentration of the solute in water, and C is a constant defined as:

$$C = g_0 \exp \left[-\frac{(\Delta H_m^S - \Delta H_m^L)}{RT} \right] \quad (5)$$

ΔH_m^S (J/mol) is the molar enthalpy of adsorption related to the first layer, ΔH_m^L is the molar enthalpy of condensation, and g_0 is the entropic factor. The BET isotherm consists of two adjustable parameters (q_m , C). Because Equation (4) did not give good fit of the experimental data, some authors proposed keeping c_s as an adjustable parameter [27,28]. In this case, there are three adjustable parameters in the BET isotherm, and the equation gives a better fit of the experimental data; however, large discrepancies between the calculated c_s and the experimental values were found. This resulted in attempts to redefine the meaning of c_s in Equation (4). For instance, Miller et al. [29] defined c_s as the concentration at which the adsorbent is saturated by adsorbate.

Ebadi et al. [30] proposed a different approach, and instead of using an ad hoc parameter such as c_s , they directly modified the BET isotherm derivation to the form expressed by Equation (6).

$$q_e = q_m \frac{K_S c_e}{(1 - K_L c_e)(1 - K_L c_e + K_S)} \quad (6)$$

K_S is the equilibrium adsorption constant for the first (adjacent) layer, and K_L is the equilibrium adsorption constant for the upper layers. These two constants define

the constant C ; $C = K_s/K_L$. This model was successfully applied for various adsorption processes, including oil adsorption [31–33].

2.3. Freundlich Isotherm (FI)

The FI was originally an entirely empirical function first proposed for a description of gas adsorption onto a solid surface but is also frequently used for adsorption from solutions. Unlike the LI, the FI is used for a description of multilayer adsorption on heterogeneous surfaces, and a non-uniform (exponential) distribution of adsorption heats is considered. Heterogeneous surfaces with a non-uniform distribution of adsorption heats can be differentiated from homogeneous surfaces by calorimetric measurements of the heat of adsorption. The heat of adsorption per mass of adsorbed solute on a homogeneous surface is constant, whereas for a heterogeneous surface, it depends on the degree of surface coverage. The Freundlich isotherm can also be derived in different ways [34,35], for instance, by attributing the change in the equilibrium constant of the binding process to the heterogeneity of the surface and the variation in the heat of adsorption [14].

$$q_e = K_F c_e^{1/n}, \quad (7)$$

$$\ln q_e = \ln K_F + \frac{1}{n} \ln c_e \quad (8)$$

where $1/n$ is the heterogeneity factor, n characterizes the intensity of the adsorption process and characterizes the relative distribution of the energy and the heterogeneity of the adsorbent reactive sites, and K_F (L/mg) is the Freundlich adsorption constant.

2.4. Dubinin–Radushkevich (D-R) Isotherm

The D-R model in general takes into account the effect of the porous structure of the adsorbents [36]. The model is based on adsorption potential theory considering that the adsorption process is related to micropore volume filling [37], and Gaussian adsorption energy distribution is considered [17]. The D-R isotherm is expressed by Equation (9):

$$q_e = q_m \exp(-\beta \varepsilon^2) \quad (9)$$

where β ($\text{mol}^2 \text{kJ}^{-2}$) is a constant related to the adsorption energy, and ε (kJ mol^{-1}) is the adsorption potential (also called the Polanyi potential). The Polanyi potential for gas adsorption corresponds to the change in the Gibbs free energy of an adsorbent after adsorption of 1 mol of gas [38].

The D-R isotherm has also been adapted for the adsorption of liquids. In this case, the term ε is defined by Equation (25), where c_s is the saturation concentration of the solute in water, similar to the BET isotherm.

$$\varepsilon = RT \ln \left(\frac{c_s}{c_e} \right), \quad (10)$$

β can be used for an estimation of the average energy of adsorption (E) by Equation (11):

$$E = 1/\sqrt{2\beta} \quad (11)$$

The D-R isotherm is often used to distinguish between physical and chemical adsorption [39,40]. It was postulated [41] that if $E \in (8.0\text{--}16.0)$ kJ/mol, then the adsorption process occurs by chemisorption, and if $E < 8.0$ J/mol, then the adsorption has physical character.

It should be mentioned at this point that the Polanyi potential is frequently used in the wrong form [22,41]:

$$\varepsilon = RT \ln \left(1 + \frac{1}{c_e} \right) \quad (12)$$

that does not respect a dimensional consistency and leads to the wrong description of experimental data, as discussed by Hu and Zhang [42].

2.5. Error Analysis

In the past a linear regression analysis has been mostly applied for analysis of experimental data obtained from the adsorption process due to its numerical simplicity. It has been used to quantify the distribution of adsorbates on sorbents and to verify the consistency of adsorption models and the theoretical assumptions of adsorption models [43,44]. However, recent studies have indicated that the error structure of experimental data is usually changed if the original nonlinear adsorption isotherms are transformed into their linearized forms [45]. For this reason, nonlinear regression analysis is currently often preferred, since it provides a mathematically rigorous method for determining adsorption parameters using the original form of isotherm equations [46,47]. The nonlinear regression includes the minimization of error distribution between the experimental data and the predicted isotherm based on its convergence criteria [48]. The most common error functions used in nonlinear analysis are summarized in Table 1.

Table 1. The most common error functions used in nonlinear analysis.

The sum of the squares of the errors (SSE)	$SSE = \sum_i^N (Q_{a\ i\ cal} - Q_{a\ i\ meas})^2$
The sum of the absolute errors (SAE)	$SAE = \sum_i^N (Q_{a\ i\ cal} - Q_{a\ i\ meas})$
The average relative error (ARE)	$ARE = \frac{100}{N} \left(\frac{Q_{a\ i\ cal} - Q_{a\ i\ meas}}{Q_{a\ i\ meas}} \right)$
The hybrid fractional error function (HYBRID)	$HYBRID = \frac{100}{N-p} \sum_i^N \left(\frac{(Q_{a\ i\ cal} - Q_{a\ i\ meas})^2}{Q_{a\ i\ meas}} \right)$
Marquardt's percent standard deviation (MPSD)	$MPSD = 100 \times \sqrt{\frac{1}{N-p} \sum_i^N \left(\frac{Q_{a\ i\ meas} - Q_{a\ i\ cal}}{Q_{a\ i\ meas}} \right)^2}$

3. Thermodynamics of Adsorption

The thermodynamic parameters of adsorption, particularly the isosteric Gibbs energy of adsorption (ΔG_{ad}^0), the isosteric enthalpy of adsorption (ΔH_{ad}^0), and the isosteric entropy of adsorption (ΔS_{ad}^0), are calculated from adsorption (equilibrium) constants, particularly from the Langmuir adsorption constant, in order to characterize the thermodynamics of adsorption at various temperatures [17]. However, the use of those constants should be made with caution. The first problem is that the equilibrium constant in the original Langmuir isotherm is not dimensionless, whereas the equilibrium constant K^0 in Equation (13) has no dimension [17].

$$\Delta G_{ad}^0 = -RT \ln K^0, \quad (13)$$

$$\Delta G_{ad}^0 = \Delta H_{ad}^0 - T \Delta S_{ad}^0, \quad (14)$$

$$\ln K^0 = \frac{\Delta S_{ad}^0}{R} - \frac{\Delta H_{ad}^0}{RT}. \quad (15)$$

Equation (15) is the van 't Hoff equation. This equation serves to calculate the thermodynamic parameters of sorption from the linear regression of the experimental dependence $\ln K^0(T)$ on $1/T$. The thermodynamic parameters are expressed in J/mol. It is evident that both terms on the right side of the Equation (15) are dimensionless, and thus, K^0 must be dimensionless as well. This means that if K_L values obtained from the LI and Equation (15) are used, then K_L must first be transformed into a dimensionless parameter. The values of K_L published in the literature have various units (L/g, L/mg, L/mol, L/mmol) [49–51], and thus, some consensus is needed on how to transform the dimensional K_L into the non-dimensional K_L . Recently, some approaches addressing this issue were proposed. The first approach is based on classical thermodynamics. The K_L value involved in the LI for gases is also not dimensionless (the unit is Pa^{-1} or its equivalent); however, if it is

used as the equilibrium constant K^0 in Equation (13), K_L is multiplied by the standard reference pressure, which is commonly 1 bar. This does not change the value of K_L but makes it dimensionless. A similar principle was applied for the K_L constant in the LI for the adsorption of liquids. Let us consider solute A in liquid phase (in solution) A (liquid) and adsorbed at sorbent A (solid). In the equilibrium $A(\text{liquid}) \leftrightarrow A(\text{solid})$, the equilibrium constant can be expressed as $K = a_{\text{solid}}/a_{\text{liquid}}$, where a_{solid} and a_{liquid} are activities in the related phase at equilibrium. The equilibrium constant of the $A(\text{liquid}) \leftrightarrow A(\text{solid})$ reaction is given by Equation (16) [52,53]:

$$K^0 = \frac{\gamma_{\text{solid}} \frac{c_{\text{solid}}}{c_{\text{solid}}^0}}{\gamma_{\text{liquid}} \frac{c_{\text{liquid}}}{c_{\text{liquid}}^0}} \quad (16)$$

where c_{solid} and c_{liquid} are the concentrations in two phases, c_{solid}^0 and c_{liquid}^0 are the same concentrations in the selected standard states, and γ_{solid} and γ_{liquid} are activity coefficients. For simplicity, in dilute solutions of nonelectrolytes, $\gamma_{\text{solid}}, \gamma_{\text{liquid}} \approx 1$. If the influence of the activity coefficients is neglected and the validity of Equation (16) is respected, the last remaining problem is the determination of values related to the standard concentrations. Unfortunately, there is no generally accepted consensus in the scientific community in the case of adsorption from liquid solutions. The simplest choice is to set standard concentrations of 1 mol/L or 1 mol/kg for both components, depending on how a concentration in equilibrium is expressed. More practically, the concentration can also be 1 mmol/L or 1 mmol/kg. In this case, c_e must also be expressed in the same units. This approach can be applicable for true solutions; however, it is not physically correct to define a standard state for emulsions in this way. Other methods that consider different standard states or just nullified the dimension have been published [54–58] and critically discussed [59].

A different approach proposed by Azizian [59] is based on the reformulation of the LI in such a way that it directly leads to a dimensionless constant. The modified Langmuir isotherm based on this assumption is expressed by Equation (17):

$$q_e = \frac{q_m K_{ML} c_e}{(c_s - c_e) + K_{ML} c_e}, \quad (17)$$

$$\frac{k_a}{k_d} = \frac{\theta_e}{1 - \theta_e} = \frac{q_e}{q_m - q_e}. \quad (18)$$

This approach gives an equilibrium adsorption constant $K_{ML} = k_a/k_d$ (Equation (18)) as the dimensionless parameter, unlike the common LI, where K_L depends on the units used (it is reciprocal to the unit in which a concentration of solute in equilibrium is expressed). Equation (17) also predicts that q_m is reached when $c_e = c_s$ instead $c_e \rightarrow \infty$ as a result of the original Langmuir isotherm (Equation (2)).

However, the introduction of parameter c_s in general into the models (including BET and D-R) is questionable. It is evident that parameter c_s , which may be significantly higher than c_e , strongly influences the values obtained from the fitting of experimental data by the modified LI. Second, this model is not applicable for substances that do not form true solutions, such as emulsions, for which the saturation state cannot be unambiguously defined. This means that the dimensionless K_{ML} would also be calculated from Equation (18) for the adsorption of emulsions because no standard state is required; however, experimental data $q_e = f(c_e)$ cannot be fitted by Equation (17) because the c_s value is undefinable for emulsions. It may be kept as an adjustable parameter, however, without any physical meaning. The modified BET isotherm (Equation (6)), as proposed by Ebadi et al. [30], looks to be a good approach for evaluating the adsorption of liquids and emulsions because (i) it is a physically plausible model that lacks the involvement of any speculative parameters, (ii) it is applicable for multilayer adsorption, (iii) it does not require the use of the constant

c_s , which is an undefinable parameter for emulsions, and (iv) it enables calculations of equilibrium constants and adequate thermodynamic parameters.

4. Kinetics of Adsorption

Kinetic models serve to estimate the duration of adsorption processes and thus to estimation the time needed for the effective treatment of liquids. In batch systems, the solute concentration in the treated liquid gradually decreases with time until it reaches equilibrium with the adsorbed species. In percolating fluid systems, the solute concentration in the treated liquid is less constant and changes after passing a filter medium. The required outlet concentration of the solute should maintain some limit values (per internal specifications).

The most common kinetic models cited in the literature are the pseudo-first-order kinetic model (PFOM) and pseudo-second-order kinetic model (PSOM) for batch systems and the Thomas model and bed depth service time (BDST) model for continuous filtration processes. For the majority of common sorbents, the adsorption process is accomplished with diffusion into the bulk medium; therefore, diffusion is a key rate-limiting step in most adsorbent/solution systems. Some diffusion models, such as Douven's model and the Weber–Morris intra-particle diffusion model, will be discussed in this regard.

4.1. Pseudo-First-Order Kinetic Model (PFOM)

The PFOM, derived by Lagergren [60], is based on the simplified precondition that the rate of adsorption is controlled by an adsorbed amount (concentration of occupied sites on the sorbent) rather than a concentration of adsorbing substances in solution. The first-order kinetics implies that one element interacts with one unoccupied reaction site on the sorbent, and this process is described by Equation (19).

$$\frac{dq}{dt} = k_1(q_e - q) \quad (19)$$

where q is the amount of adsorbed species per mass of adsorbent (mg/g), k_1 (min^{-1}) is the pseudo-first-order rate constant, q_e is the amount of adsorbed species per mass of adsorbent in equilibrium (mg/g), and t is time (min). An integrated form of Equation (1) gives Equation (20):

$$q = q_e(1 - e^{-k_1 t}), \quad (20)$$

which enables the determination of parameters q_e and k_1 from nonlinear fitting. On the other hand, the linear form given by Equation (21) is mostly applied and cited in the literature.

$$\ln(q_e - q) = \ln q_e - k_1 t, \quad (21)$$

$$q_e = \frac{(c_0 - c_e)V}{m} \quad (22)$$

where c_0 (mg/L) is the initial concentration, c_e (mg/L) is the concentration in equilibrium, V (L) is the volume of the investigated liquid and m (g) is the mass of the sorbent. The units mentioned here are the most common units referred to in the literature, but different units can be used as well.

4.2. Pseudo-Second-Order Kinetic Model (PSOM)

The PSOM represents the most common model for a quantitative description of the sorption rate of substances onto sorbent media [61,62]. The PSOM is expressed by the second-order differential equation (Equation (23)):

$$\frac{dq}{dt} = k_2(q_e - q)^2 \quad (23)$$

where k_2 is the pseudo-second-order rate constant. Unlike k_1 , which has always the dimension reciprocal to time, the constant k_2 may have various dimensions (mg/g.min, g/g.min, mmol/g.min, etc.), depending on the definition of q [20,63].

Analytical solutions of Equation (23) can be expressed in various forms [64]; however, the most common solutions are given by Equations (24) and (25), which serve for a nonlinear (Equation (24)) and linear (Equation (25)) fitting of experimental data and a calculation of q_e and k_2 .

$$q = \frac{k_2 q_e^2 t}{1 + k_2 q_e t} \quad (24)$$

$$\frac{t}{q} = \frac{1}{k_2 q_e^2} + \frac{t}{q_e} \quad (25)$$

One of the crucial assumptions for a derivation of the PSOM is that an initial concentration of bulk solution should not change significantly during sorption in order to evaluate the experimental data correctly [65]. On the other hand, this requirement is in direct contradiction to a common practice to determine q and q_e from changes in the bulk concentration (c_e), particularly in batch systems, where the initial concentration changes significantly over the sorption experiment.

Azizian [43] proposed the general kinetic model, in which the adsorption rate is described by (i) a fraction of vacancies (available reaction sites) at the surface of the sorbent ($1-\theta$), (ii) a concentration of solute in solution (c) in time t , and (iii) the desorption rate, which is given by a fraction of occupied sites at a sorbent surface (θ , where $0 \leq \theta \leq 1$) [66].

The general differential equation of that model is expressed in the form Equation (26):

$$\frac{d\theta}{dt} = k_a(c_0 - \beta\theta)(1 - \theta) - k_d\theta \quad (26)$$

where $c = c_0 - \beta\theta$, $\beta = \frac{mq_m}{M_w V}$, or $\beta = \frac{c_0 - c_e}{\theta_e}$.

c_0 is the initial molar concentration of the solute, q_m is the maximum sorption capacity of the adsorbent, M_w (g/mol) is the molar weight of the solute, V (L) is the volume of the solution, c_e is the equilibrium molar concentration of the solute and θ_e is the equilibrium coverage fraction. From the general model (Equation (26)), Azizian derived the PFOM (Equation (20)) and PSOM (Equation (25)) as special cases of the general model (Equation (26)).

Both models describe experimental data for both low and high solute concentrations, highlighting that the sorption process at high initial concentrations obeys PFO kinetics, while the PSO model better describes the sorption kinetics at lower initial concentrations [43,67–69].

Various authors have analyzed a description of experimental data widely published in the literature by the PFOM and PSOM, and they identified the following problems, which indicate doubts about the general applicability of these models without considering additional phenomena [64,66–70]: (i) unoccupied sites can be incapable of reacting with adsorbing entities independently, (ii) adsorption processes can take significantly longer than expected (electrostatic interactions between the surface and sorbents occur instantaneously and the diffusion layer at the solid/liquid interface is thin enough), and (iii) the initial concentration of substances in solution changes significantly during the experiment, particularly in the case of batch systems. More details about the limitations of the PSOM can be found in Hubbe's review [64].

Regarding the applicability of the PSO and PFO models to experimental data, Canzano [71] pointed out that the correlation between data and models characterized by R^2 values strongly depends on the selection of data. If the data set does not include enough values related to the short duration of the experiment but consists of many more data for long periods, the long-term data have a higher weight on the statistical parameters. Canzano [71] showed that the PSO model better fits data including measurements from systems that approach an equilibrium. Another problem where mathematical procedures

can overlap the physical reality is associated with a selection of the equation used from a fitting. As mentioned above, an integrated form of Equation (5) can be expressed by four different equations. It was shown that application of those equations to the same set of data leads to significantly different R^2 values in the range from 0.862 to 1. On the basis of this finding, the authors proposed, first, to minimize the number of data points nearest to equilibrium and, second, to use nonlinear fitting by Equation (24) [71].

4.3. Diffusional Models

4.3.1. Douven's Model

Diffusion is a key rate-limiting step in most adsorbent/solution systems unless the surfaces are smooth and impervious; therefore, this phenomenon has to be taken into account in the majority of sorption processes [48].

Douven's model [72] represents a generalization of Crank's model [73] based on the analytical solution of 2nd Fick's law with some preconditions such as (i) the formation of a boundary layer at the solid/liquid interface, (ii) the reversible adsorption of solutes, (iii) the continuous occurrence of adsorption during the diffusion process, and (iv), an effective diffusion coefficient is considered instead a "true" diffusion coefficient, taking into account a decrease in the rate of diffusion due to solute immobilization on the adsorbent surface. Douven's model is generally expressed by Equation (27):

$$\frac{n(t)}{n_e} = 1 - \frac{6}{\pi^2} \sum_{i=1}^{\infty} \frac{1}{i^2} \exp\left(-\frac{i^2 D_{\text{eff}} \pi^2 t}{R_p^2}\right) \quad (27)$$

where $n(t)$ is the total number of adsorbed entities at time t , n_e is the total number of adsorbed entities at equilibrium, D_{eff} is the effective diffusion coefficient, and R_p is the radius of the adsorbed entity.

Douven also developed the procedure for data analysis based on the experimentally determined half-times ($t_{1/2}$) needed for an adsorption of half of the full adsorbent capacity and showed that the PSO model is equivalent to Equation (28):

$$\frac{n(t)}{n_e} = \frac{\frac{t}{t_{1/2}}}{1 + \frac{t}{t_{1/2}}} \quad (28)$$

4.3.2. Weber–Morris Intra-Particle Diffusion (IPD) Model

The IPD model [74] is the most frequently applied model for systems in which adsorption is accomplished by the diffusion process and is described by Equation (29):

$$q = k_{\text{ipd}} \sqrt{t} + C \quad (29)$$

where k_{ipd} (mg/g.min) is the rate constant for intra-particle diffusion, and C (mg/g) is a constant related to the boundary layer thickness. This model does not distinguish among various processes that can simultaneously occur during solute sorption and considers just a single rate-limiting process of diffusion.

4.4. Adsorption Kinetics in Flow-through Systems (Fixed Bed Adsorption)

When contaminated fluid moves through a fixed bed, the pollutant to be adsorbed transfers from the bulk fluid to the adsorbent bed. Several steps are involved in the overall adsorption process of a single molecule of pollutants:

1. A mass transfer from the bulk of the fluid to the surface of the adsorbent through the boundary layer around the particle.
2. An internal diffusion through the pores of the adsorbent.
3. An adsorption onto the surface of the adsorbent.

In wastewater treatment applications, the overall adsorption process is dominated by mass transfer, especially by an intra-particle mass transfer (Figure 4), dependent on the morphology of sorbents.

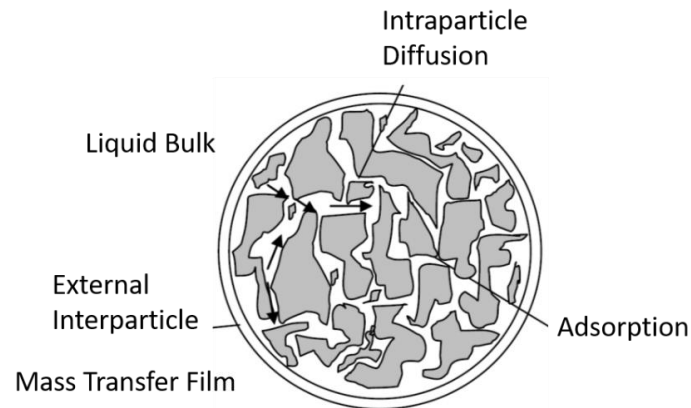


Figure 4. Steps involved in the overall adsorption process (adapted from: Muftah H. El-Naas [16]).

During a continuous adsorption process in a fixed bed, the bed can be divided into three distinguished zones in (i) the saturated zone, (ii) the adsorption zone, and (iii) a clean zone in which the adsorbent contains little or no adsorbed pollutant (Figure 5). The size and location of these three zones within the bed change with time. When the concentration of pollutant on the bottom part of the filtration column reaches some critical level of saturation, concentrations of pollutants in an effluent are higher than the required value. This point is called the *breakthrough* point and the corresponding curve of pollutant concentration in the effluent versus time is called the *breakthrough curve*. In this phase, the filtration process is stopped and the adsorption medium is cleaned. Otherwise, the concentration of pollutant in effluent rapidly increases until it reaches an exhaustion point when the column approaches saturation, and the effluent releasing the bed has the same concentration of pollutant as the influent stream.

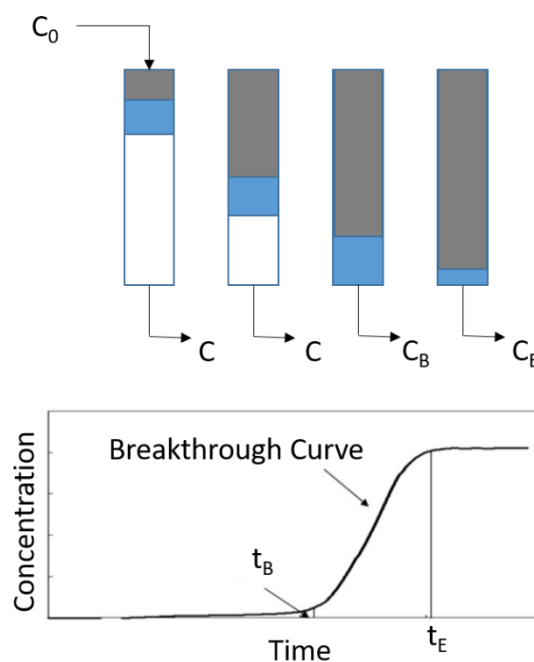


Figure 5. A schematic representation of the movement of the adsorption zone and the related breakthrough curve (adapted from: Muftah H. El-Naas [16]).

The performance of column breakthrough can be analyzed based on the Henry C. Thomas model (Equation (30)) [75,76], which was originally developed for solute chromatography. This is one of the most utilized models for evaluating column performance and can be applied for a prediction of adsorption kinetics and the adsorption capacity in flow-through systems [77]. In this model, the intra-particle diffusion during the mass transfer process is considered to be negligible.

$$\frac{C_e}{C_0} = \frac{1}{1 + \exp\left[\frac{k_{th}}{Q}(q_m M - C_0 V)\right]} \quad (30)$$

Equation (30) can be expressed in linear form as Equation (31):

$$\ln\left(\frac{C_0}{C_e} - 1\right) = \frac{K_{th} q_m M}{Q} - \frac{K_{th} C_0 V}{Q} \quad (31)$$

where C_0 is the feed concentration (mg/L), C_e is the column effluent concentration (mg/L), K_{th} is the kinetic rate constant (L/(mg.min)), q_m is the adsorption capacity of the column (mg/g), M is the mass of media in the bed (g), V is the column effluent volume (L) and Q is the feed flow rate (L/min). The breakthrough data can be fitted by plotting $\ln\left(\frac{C_0}{C_e} - 1\right)$ versus V ; q_m and K_{th} can be determined depending on the intercept and slope [78].

Pintor et al. [79] developed the model given by Equation (32)a,b,c for testing the adsorption of oil from oil/water emulsions.

$$(a) \ q = \frac{K_f c_{b0}}{1 + \xi_m} \left[1 - \exp\left(-\frac{(1 + \xi_m)t}{\xi_m \tau_f}\right)\right] \quad (b) \ \xi_m = \frac{WK_p}{V} \quad (c) \ \tau_f = \frac{1}{K_f a_f} \left(\frac{\varepsilon_b}{1 - \varepsilon_b}\right) \quad (32)$$

where c_{b0} (mg/L) is the initial concentration of oil in the bulk solution, ξ_m is the batch capacity factor, τ (s) is the time constant characterizing diffusion through a boundary layer, V (L) is the volume of the solution (a volume of a reactor), ε_b is the bulk porosity, K_f (cm/s) is the mass transfer coefficient of the boundary layer, and a_f (cm²/cm³) is the external surface area of sorbent per volume of sorbent given by the relation $a_f = 3/r_p$, where r_p (cm) is the particle (sorbent) radius. The adjustable parameters τ_f and K_f are obtained from a fit of experimental data by Equation (32).

4.5. Bed Depth Service Time (BDST) Model

The BDST model predicts a dependence of the service time (t_b (min)) at the breakthrough point in the depth (X , (cm)) of the packed column. In this model, intra-particle diffusion is neglected, and direct adsorption of solutes on the adsorbent surface is assumed. The original BDST model was proposed by Bohart et al. [80] in the following form (Equation (33)):

$$\ln\left(\frac{c_0}{c_b} - 1\right) = \ln\left[\exp\left(\frac{k_{ads} N_0 X}{v}\right) - 1\right] - k_{ads} c_0 t_b. \quad (33)$$

Hutchins [81] proposed a linearized form of that model, expressing a direct relation between t_b and X by Equation (34).

$$t_b = \frac{N_0 X}{c_0 v} - \frac{1}{k_{ads} c_0} \ln\left(\frac{c_0}{c_b} - 1\right). \quad (34)$$

N_0 (mg/L) is the dynamic bed capacity, v (cm/h) is the linear flow rate, defined as the ratio of the volumetric flow rate Q_{vol} (cm³/h) to the cross-sectional area of the bed, S_c (cm²); c_0 and c_b (mg/L) are the initial and breakthrough concentrations of the solute, respectively, and k_{ads} (L/mg.h) is the adsorption rate constant.

From a practical point of view, the breakthrough curves can be described using various commercial and non-commercial software. For example, freely available software FAST,

Fixed-bed Adsorption Simulation Tool () is the program for the prediction of breakthrough curves of fixed-bed adsorption filters used in water treatment. Inputs include an empty bed contact time, mass of adsorbent, bed porosity, particle density, particle diameter, influent concentration, flow rate, bed volume. The outputs are Freundlich isotherm parameters, film diffusion coefficient (m/s), surface diffusion coefficient (m²/s), breakthrough curve, solute distribution parameter (Dg), Biot number (Bi), and Stanton number (St).

Some examples of the separations of o/w emulsions as well as mostly used models are shown in Table 2.

Table 2. The models used for sorption of oil by the use of various materials.

Sorbent	Emulsion	Outputs	Models	Ref.
Optipore L493, Lewatit AF5, Amberlite IRA958 (synthetic resins), batch system	Synthetic PW emulsion, Octane 95, nonionic surfactant, 25–50 ppm	Below 2 ppm	Langmuir, Freundlich, Flor–Huggins isotherms, Toth, Dubinin–Radushkevich isotherms, PFO, PSO models, intra-particle diffusion model	[19]
Calcium alginate hydrogel modified by maleic anhydride, batch system	Crude oil, sonication, no surfactant, 1 M NaCl, 100–500 ppm	80% removal efficiency	Freundlich, BET isotherms, PFO and PSO models, intra-particle, diffusion model	[33]
Fe ₃ O ₄ magnetite nanoparticles grafted in silica (SiO ₂), batch system	Gasoline oil, 500–4000 ppm	>90% removal efficiency	Langmuir, Freundlich isotherms	[82]
Iron Oxide/ Bentonite Nano Adsorbents, batch system	Diesel oil, 66 to 170 ppm, non-ionic surfactant	67% removal efficiency	Langmuir, Freundlich, Toth	[83]
Thermally reduced graphene and graphene nanoplatelets, batch system	200 ppm and adjusted salinity	TRG: 1550 mg oil/g GNP: 805 mg oil/g	Langmuir, Freundlich, Dubinin–Radushkevich, Tempkin isotherms	[84]
Zeolitic imidazolate, batch system	Soybean oil, 5 wt%	6633 mg/g	Langmuir, Freundlich isotherms, PFO and PSO	[85]
Hydrophobic silica aerogels, batch system	Vegetable oil, motor oil 10W30, light crude oil, Tween 80		Freundlich isotherm	[86]
https://www.sciencedirect.com/topics/biochemistry-genetics-and-molecular-biology/lanthanum (accessed on 26 February 2021), zirconium and cerium embedded chitosan/gelatin, batch system	4 wt% cutting oil		Langmuir, Freundlich, Dubinin–Radushkevich, Tempkin isotherms	[87]
Activated carbon, bentonite, deposited carbon, batch system	Produced wastewater from Gamasa Petroleum Company, 600–1012 ppm	Up to 98% removal efficiency	Langmuir, Freundlich isotherms	[88]
Polyether polysiloxane, batch system	Oil-flooding-produced water from the Daqing oil field, 400 ppm	90% removal efficiency	Langmuir, Freundlich isotherms	[89]

Table 2. Cont.

Sorbent	Emulsion	Outputs	Models	Ref.
Regranulated cork, flow system	Sunflower oil and saponified matter, 200 ppm	<15 ppm	Freundlich isotherms and linear partitioning models	[79]
Magnetic nanosorbent polydimethylsiloxane, zinc oxide, batch system	2 wt% diesel, span 80	96% removal efficiency	PFO and PSO, intra-particle diffusion models	[90]
Hydrophilic hierarchical carbon with TiO ₂ nanofiber membrane, batch system	Engine oil, cooking oil, hexane, toluene, 1000 ppm, Surfactant SDS 200 ppm	95.4% removal efficiency	BET isotherm	[91]
Sunflower pith, flow system	Artificial reservoir brine, 0.1, 2.0, and 20.0 g/L of oil	Over 99% removal efficiency	PFO, PSO, Modified logistic model	[92]
Magnetic ZnFe ₂ O ₄ -Hydroxyapatite Core-Shell Nanocomposite, flow system	Produced water containing oil from 100 to 10,000 ppm	98% removal efficiency	Thomas-BDST model, Yoon-Nelson model	[93]
Oleophilic natural organic-silver nanocomposite, batch system	Motor oil, 200–1000 ppm	NA	Langmuir, Freundlich, Temkin isotherms, PFO and PSO	[94]
Chitosan/Mg-Al hydroxide composite, batch system	4 wt.% cutting oil	78% removal efficiency	Langmuir, Freundlich, Dubinin-Radushkevich, Tempkin isotherms	[95]

5. Interfacial interactions and Wettability of Surfaces

The physical parameter that describes energy/force-related phenomena that act on the outer surface of a material or at the interface between adjacent bodies is called the specific free surface energy (σ (J/m²)) or the surface tension (γ (N/m)). Except for intramolecular (covalent, ionic) bonds, intermolecular interactions, generally called Van der Waals interactions, contribute to both internal and interfacial energy. The energy of those interactions strongly decreases with the distance between interacting bodies ($\sim 1/r^6$) and with temperature ($1/T$) [17]. The range of the forces is approximately from 0.15 to 1 nm, and the energy depends on the type of interactions: (i) dipole-dipole interactions ~ 5 to 25 kJ/mol, hydrogen bonds ~ 10 to 40 kJ/mol, (ii) ion-dipole interactions ~ 40 to 600 kJ/mol, (iii) ion-induced dipole interactions ~ 2 to 10 kJ/mol, and (iv) London (dispersion) interactions ~ 0.5 to 40 kJ/mol. These interactions are time-independent and act instantaneously; therefore, the time dependence of an adsorption process is governed by additional, mostly diffusional phenomena [96].

The most common approach for characterizing interfacial tension is based on the sessile drop method, which is a measurement and evaluation of the contact angles of liquids on a solid surface at equilibrium at room temperature and atmospheric pressure. In a sense of water/oil separation, not only are solid/oil/air interfaces but also mostly solid/oil/water interfaces investigated, and related contact angles at different interfaces indicate the suitability of separation methods for different morphologies of oil/water systems (emulsions, free oils). The typical features of the wettability of smooth and rough surfaces by oil-in-water surroundings are briefly described below.

5.1. A Droplet Placed at a Smooth and Rough Surface in Air

The fundamental dependence between the equilibrium contact angle and related surface tensions is given by Young's equation (Equation (35)), which describes the equilibrium

state of a small droplet of pure liquid deposited on a uniform, smooth and non-penetrating surface [97–100]:

$$\gamma_{SV} - \gamma_{SL} = \gamma_{LV} \cos \Theta \quad (35)$$

where Θ is the contact angle, γ_{SV} is the interfacial tension at the solid–vapor interface, γ_{SL} is the interfacial tension at the solid–liquid interface, and γ_{LV} is the surface tension of the liquid, which is in equilibrium with a saturated vapor phase.

Other types of surfaces are those that have a fine roughness (surface is interrupted by cavities with sharp edges having micro/nano inter-cavity distances); therefore, those cavities are not wettable by liquids but are filled with air. This case is called the Cassie state and is characterized by the Cassie and Baxter equation (Equation (36)) [101]:

$$\cos \Theta^* = f \cos \Theta + f - 1 \quad (36)$$

where f is the fraction of the solid surface that is in contact with the liquid. The assumption involved in Equation (36) is that the contact angle of the droplet at the air layer is 180° . The Cassie state corresponds to the very low adhesion between liquid and solid, and therefore is usually unstable.

The transition between the Wenzel case and the Cassie–Baxter case depends on both the chemical character of the surface and the geometry of the roughness, particularly the scale of the roughness (Figure 6). Microscale roughness leads to strong contact angle hysteresis effects. Contact angle hysteresis cannot be determined directly but can be characterized via the measurement of advancing and receding contact angles. The contact angle hysteresis is defined as the difference between the advancing contact angle (ACA) and the receding contact angle (RCA) of a droplet that moves on the tilted surface. The differences between static sliding angle (SSA) and dynamic sliding angle (DSA), similar to those between ACA and RCA, may range from a few degrees to a few tens of degrees, and $SSA > DSA$ [102,103]. The relation between the contact angle hysteresis and sliding angle is described by the Furmidge equation (Equation (37)) [38]:

$$\frac{mg \sin \alpha}{w} = \gamma_{LV} (\cos \Theta_{\text{rec}} - \cos \Theta_{\text{adv}}) \quad (37)$$

where m is the weight of a droplet, α is a sliding angle, w is the width of the droplet, and Θ_{adv} and Θ_{rec} are advancing and receding contact angles, respectively.

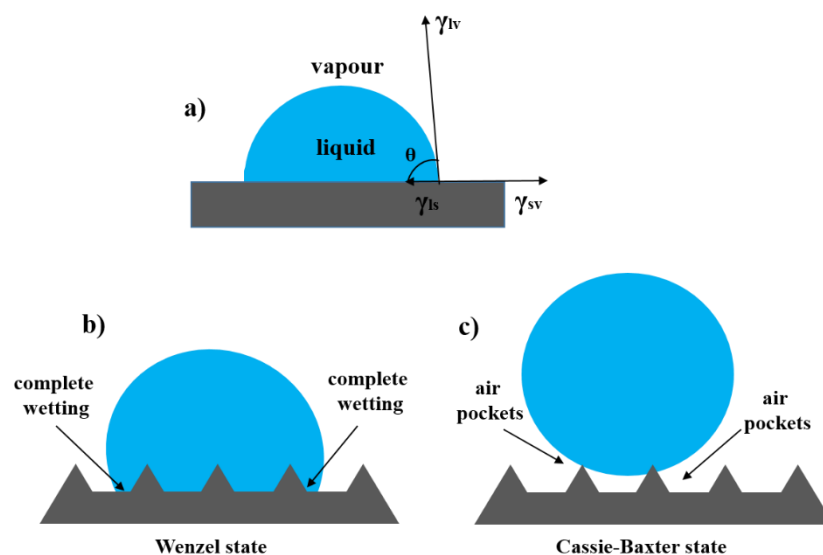


Figure 6. Schematic diagrams of a liquid droplet on various surfaces. (a) Flat surface, (b) Wenzel state, (c) Cassie–Baxter state.

5.2. A Droplet Placed at a Smooth and Rough Surface in Water

In this case, the wettability of surfaces by oil is significantly influenced by the contribution of the surface tension of water because, unlike air, which has no surface tension, water has one of the highest surface tension values (~72 mN/m) [104–106]. In this case, considering a three-phase solid substrate (S)/oil (O)/water (W) system, Young’s equation can be rewritten into the forms given by Equations (38)–(40) [107]:

$$\cos \Theta_W = \frac{\gamma_{SW} - \gamma_{SA}}{\gamma_{WA}}, \tag{38}$$

$$\cos \Theta_O = \frac{\gamma_{SO} - \gamma_{SA}}{\gamma_{OA}}, \tag{39}$$

$$\cos \Theta_{OW} = \frac{\gamma_{OA} \cos \Theta_O - \gamma_{WA} \cos \Theta_W}{\gamma_{OW}} \tag{40}$$

where γ_{OA} , γ_{WA} , and γ_{OW} are the oil/air, water/air, and oil/water interface tensions, respectively, and Θ_O , Θ_W , and Θ_{OW} are the contact angles of oil in air, water in air, and oil in water, respectively. Equations (38)–(40) indicate that a hydrophilic surface in air is also oleophilic in air because $\gamma_{OA} \ll \gamma_{WA}$, and hydrophilic surfaces in air behave as oleophobic in water, as is evident from Equation (40) [107].

If the roughness of a surface is considered, then equations for the Wenzel state and Cassie state can be used to describe the surface wettability using Equations (41) and (42):

$$\cos \Theta_{OW}^* = r_w \cos \Theta_{OW}, \tag{41}$$

$$\cos \Theta_{OW}^* = f \cos \Theta_{OW} + f - 1 \tag{42}$$

where Θ_{OW}^* and Θ_{OW} are the contact angles on the oil droplet on the rough surface and the smooth surface in the water surroundings, respectively. The Wenzel state corresponds to the situation where an oil droplet is attached to a rough, superhydrophobic surface, which has pores filled with air, and capillary forces are strong enough to suck adjacent oil into the pores [106]. In this case, the surface is fully wetted by oil. The Cassie state corresponds to the situation where valleys on the surface are filled with water, which suppresses the penetration of oil into those cavities, and oil droplets can only be in contact with the “pin” objects. This situation leads to an enhanced oleophobicity of such surfaces [107]. The capability or incapability of water to fill cavities at a given surface plays an important role in the final wettability of the surface by oil. This capability is given by the surface free energy and surface topology. Superhydrophobic surfaces are characterized by a static contact angle of water of over 150°, and the rolling angle is below 6–10°. Superhydrophobic or superoleophilic behavior is a consequence of a combination of the chemical structure of the material and controlled roughness [108–111].

The above considerations are summarized in Figure 7 [52].

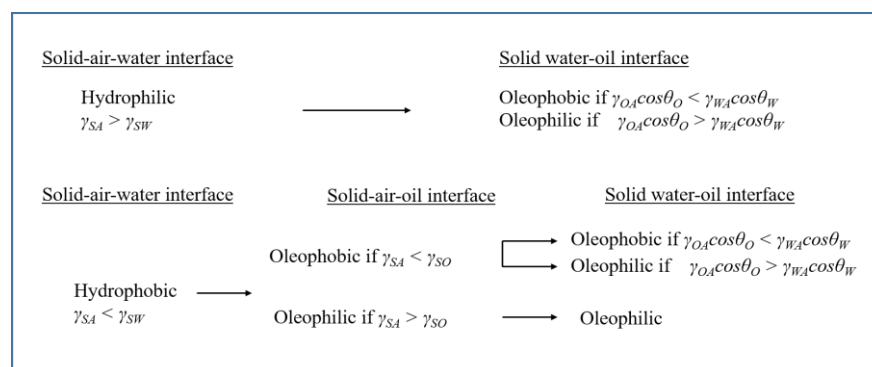


Figure 7. Summary of “Phylic”/“Phobic” natures at various interfaces.

6. Oil/Water Separation Techniques according to the Wettability of Solid/Oil/Water Interfaces

6.1. Free (Stratified) Oil Separation from Water (Oil Spills): Superhydrophobic and Superoleophilic Surfaces

This treatment is applicable for the separation of free oil (oil spills) through sorption. For this reason, various types of particles, mats and bulk polymeric sorbents have been treated and tested [2,3,112]. Surface modification is mostly performed on traditional sorbents such as powders (silica, clays, activated carbon, ground cellulose-based bio-waste including kapok, wood dust, kenaf, etc.), synthetic polymer fabrics (polypropylene), and polymer sponges (polyurethane, melamine, synthetic rubbers, etc.). Surface treatment improves soil sorption and reduces water permeability into the materials [106].

6.2. Oil/Water Emulsions—Separation of Oil Droplets by Membrane Filtration. Superoleophobic and Superhydrophilic Surfaces

Ultra- and microfiltration technologies, which use suitable membranes, are commonly employed for oil/water emulsion separation. The drawback of membrane filtration is associated with intensive fouling of their surfaces, which leads to a decrease in the flow rate through the membranes and enhances the time and cost needed for cleaning. Designing membranes with superoleophobic and superhydrophilic surfaces enables suppression of that unfavorable behavior. From a chemical point of view, materials should have a surface free energy in the range from 20–30 mN/m (common values for oils) to ~72 mN/m (surface tension of water) and characteristic dimensions ranging from several tens to hundreds of microns. The low surface tension of materials is given by their composition; among the materials with the lowest surface energy are polydimethylsiloxane (19.8 mN/m), polytetrafluoroethylene (22.6 mN/m) and polypropylene (29.6 mN/m), which means materials where the cohesion energy is given by London dispersive forces. The roughness can be introduced into membranes through various physical, chemical and processing approaches [38,104–107]. The Cassie wetting state corresponds to this filtration mechanism.

6.3. Oil/Water Emulsions—Separation of Oil Droplets by Sorption (Preferable in Batch Systems). Superhydrophobic and Superoleophilic Surfaces

Strategies similar to those for the separation of free oil from water can also be applied for the separation of O/W emulsions in batch systems. The oil component adsorbs at the sorbent surface and, in some cases, penetrates into the bulk structure, where it is localized at the internal surface of sorbents. The separation efficiency is given by the surface area available for sorption. Once a surface area is fully covered, the separation process stops. The Wenzel wetting state corresponds to the situation where the oil droplet is attached to a rough, superhydrophobic surface, which has pores filled with air, and capillary forces are strong enough to suck adjacent oil into the pores. In this case, the surface is fully wetted by oil, and the surface and adjacent pores are fully utilized for oil sorption.

6.4. Oil/Water Emulsions—Separation of Oil Droplets by Demulsification-Coalescence (Deep-Bed Filtration). Balanced Hydrophobic and Oleophilic Surfaces

Two basic filtration media for deep-bed filtration are used in industry. The first type of medium includes fibrous, porous woven and nonwoven mats. If the dominant mechanism of oil separation is demulsification via coalescence, these media are called coalescers. The majority of commercial coalescers separate droplets with diameters less than 100 μm , and if they are formed by a combination of different fibrous mats that vary in composition, thickness, and pore size, they can separate droplets smaller than 10 μm [113–117].

The separation of droplets smaller than 10 μm is a challenging task because small droplets behave as solids due to the high internal Laplace pressure and have a small contact area with fibers within mats; therefore, coalescence occurs insufficiently. An improvement of fibrous coalescers is based on the design of sandwich structures formed by a combination of different mats varying in the type of material, fiber thickness, pore size, and specific surface treatment, leading to tailored surface porosity and roughness [113–117].

The second type of medium for deep-bed filtration includes various organic, synthetic and inorganic granules, possessing roughly spherical shapes and sizes on the order of millimeters. All these media adsorb oil to various extents, and if the surface chemistry and topology are favorable, they initiate coalescence of oil droplets at their surfaces and therefore significantly contribute to the separation efficiency [118]. If coalescence is promoted at the filter surface, the droplets, which are attached within a short mutual distance for some time, have favorable conditions to merge with each other. Agarwal et al. [119,120] tested the adhesion of droplets of iso-octane on surfaces of different polarities (the surface free energy), porosities, and roughness and searched for suitable conditions, which led to the efficient coalescence of such small droplets. The work of adhesion (Equation (43)) is considered the parameter characterizing the ability of droplets to be attached onto a surface and to remain there for some time. The dependence of the work on adhesion on the surface free energy of the filler is shown in Figure 8.

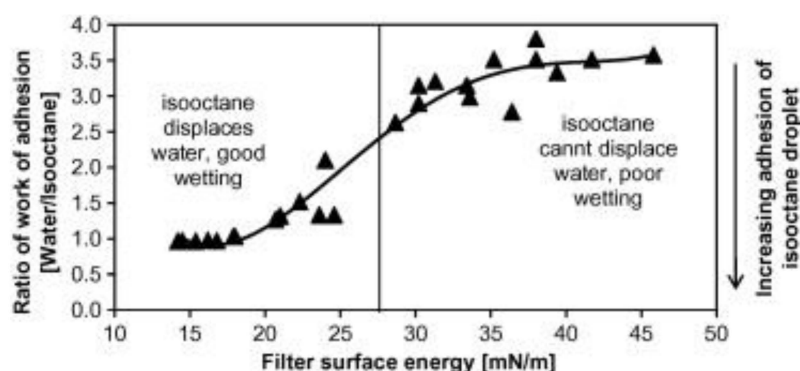


Figure 8. Influence of the solid surface energy on the work of adhesion and wetting of iso-octane and water.

The work of adhesion (W_{ad}) between different phases can be calculated by the Young–Dupre equation (Equation (43)) [119]:

$$W_{ad} = \gamma_{Ly}(1 + \cos \Theta_{Ly}) \quad (43)$$

where γ_{Ly} is the interfacial tension between the dispersed liquid (y-oil) and the surroundings (water, or y-air). The dependence of the ratio of W_{ad} (water/iso-octane) on the surface energy has a sigmoidal character, and the curve characterizes two distinguished regions: the region with low surface energy in which the adhesion of iso-octane droplets is stronger than the adhesion of water (below ~25–27 mN/m) [119] and the region with high surface free energy (over 30 mN/m) where the adhesion of water is stronger than the adhesion of oil. Materials with high-energy surfaces are not suitable for oil adsorption because they cannot replace adsorbed water. For this reason, the surfaces of coalescing media should be hydrophobic and oleophilic, which enable good wetting and sufficient contact time, thereby promoting the coalescence of droplets [119].

The second important point is the morphology of the surfaces, characterized by roughness (quantified by a dimensionless roughness factor) and porosity (quantified by the pore size in nm/ μ m). As discussed above, the surface topology enhances the intrinsic wettability of flat surfaces. However, these effects may not be favorable for droplet coalescence. Agarwal et al. [119] demonstrated that nanoscale roughness improves oil droplet spreading and adhesion at hydrophobic surfaces (Wenzel wetting), while nanocoated hydrophilic surfaces lead to an enhanced contact angle and improved mobility, characterized by low static and dynamic sliding angles (Cassie state) in water surroundings (Figure 9). This effect may also contribute to emulsion formation, however, outside the solid surface, which takes a long time, especially for diluted, stabilized emulsions, and the separation efficiency is low. The Wenzel state enhances the probability of mutual

contacts between oil droplets at a surface with high coalescence and separation efficiency. A pore size of cavities larger than the drop size, as well as high roughness, is favorable for coalescing media. On the other hand, oil absorption within porous oleophilic media is not favorable for coalescence [119].

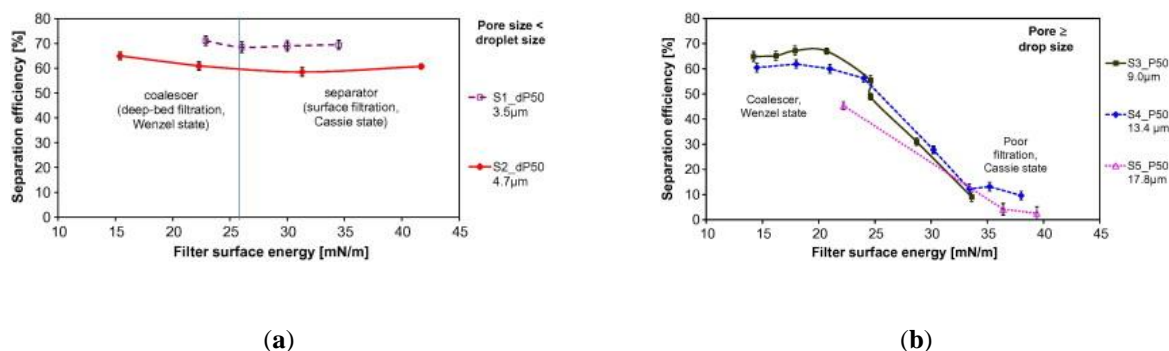


Figure 9. Influence of substrate surface energy on oil-in-water emulsion separation performance for (a) pore size < dispersed droplet size, pressure drop 2.2 bar and (b) pore size \geq dispersed droplet size, pressure drop 1.1 bar.

The same authors in another paper [120] demonstrated those findings on woven and nonwoven fabrics treated by silica nanoparticles, and the influence of the fabric thickness, fiber diameter, porosity, pore size, and microscale roughness were systematically investigated. The best configurations enabled the separation of emulsions consisting of oil droplets with a diameter of 5 μm , with a separation efficiency of 80% at a pressure drop of 160 mbar and a superficial velocity of approximately 1.0 m/min.

The physical and chemical principles discussed above are the same for both fibrous coalescers and granular media; however, there are some differences resulting from different media geometries. First, the interstices (pores) between fibers in mats are much smaller than the interstices (free volume) in the bed formed by granules. From simple geometry it can be estimated that the pore size has the same order or one order of magnitude less than the diameter of fibers/granules. Common fabrics have pore sizes on the order of 100–101 μm , whereas pores within granular beds have a size of 100 μm . The smaller space is more favorable for coalescence, which can occur at a surface and in a solution; however, on the other hand, the space is filled faster with residual droplets, which leads to the pressure drop. For the granular bed, because the space of interstices is relatively large, coalescence proceeds at the surface of granules only. The advantage is a lower influence on the pressure drop and a less intensive backwashing procedure [121,122].

Granular nutshells, particularly walnut shells, are the most common media in the petrochemical industry for oil impurity removal from produced water. These filters are considered the standard technology, mainly for onshore use. The separation mechanisms include oil adsorption on the surface and coalescence. It was shown that droplets act at first as discrete particles, which are trapped by straining, and then the process continues by coalescence of those larger droplets, leading to the formation of large pools of oil localized within the filter interstices. An oil emulsion (unrefined Bakken crude oil; 100 ppm) was filtered through the bed (a height of 23 inches and diameter of 4 inches) over six hours. It was found that 95% of the oil was trapped in the first 12 inches of the bed and 99% in the first 18 inches of the bed. Large pools of coalesced oil were detected within the medium interspace [118].

Coalescing agents [123] have been used in deep-bed filtration using sand [124] and sawdust [125] as the filter media. Cetyltrimethylammonium bromide as a coalescing agent has been added for the separation of hexadecane/water emulsions by using a quartz sand bed packed in a Plexiglas column with an inner diameter of 2.5 cm and a length of 10 cm [124]. An n-hexadecane/water emulsion at a concentration of 1000 ppm was pumped from the bottom at a superficial velocity of 0.04 cm/s using a peristaltic pump. It was concluded that the deposition of oil is found to be a maximum at a cetyltrimethylam-

monium bromide concentration of 5×10^{-6} M, at which the sand surface has an opposite charge to that of the emulsion droplets. Below this concentration, the deposition efficiency is reduced due to the electrostatic repulsion between the negatively charged droplets and the sand. Above this concentration, the deposition is again reduced due to the surfaces of sand and droplets being positively charged.

The coagulator calcium sulfate has been used to promote coalescence of oil/water emulsions at a concentration of 24 ppm in deep-bed filtration experiments. The filter media consist of sawdust with heights ranging from 30 to 55 mm packed in a 20-cm column, with the inner glass tube replaced by a 26-mm diameter methacrylate column. The dissolved salt ions compress the electric double layer around droplets, neutralize repulsive forces among them and between droplets and sawdust particles and hence enhance the coalescence of oil droplets. Moreover, the lack of electrostatic repulsion improves the physical adsorption of the oil droplets on the sawdust surface, originally negatively charged. Therefore, the oil droplet size is increased, and its charge is neutralized so that the disperse phase can be retained in the filter media interstices [125].

7. Conclusions

This review concerns the mechanisms of a separation of emulsified water/oil mixtures and it covers the (i) kinetics of adsorption, (ii) adsorption isotherms, (iii) interfacial interactions, and (iv) water/oil separation techniques based on the wettability of solid/oil/water interfaces. The advantages and drawbacks of commonly used as well as newly proposed kinetic and adsorption models were reviewed, and their applicability for the characterization of oil/water separation was discussed. It was pointed out that the direct applicability of models that can be applied to describe the sorption process from true solutions is not straightforward, and these models should be used with caution, especially if equilibrium constants of adsorption and related thermodynamic parameters are estimated. The wettability of solid sorbents by oil within a water environment was discussed for both smooth and rough surfaces. The main focus was on the surface energy and surface topology of solid media and their influence on the coalescence separation mechanism.

The separation of emulsions through deep-bed filtration is a complex technological process, and, therefore, not all aspects of this technology were covered in this review. Among those mechanisms were transport mechanisms include straining, interception, inertia, sedimentation, hydrodynamic action, filter and flow orientation, flow velocity, pressure drop, etc. Some relevant references concerning those areas were mentioned. For theoretical models that address the description of different phenomena related to the oil/water emulsion separation processes, let us mention just one aspect here that deserves attention in the future: the lack of suitable adsorption isotherms that can be correctly applied for a description of oil adsorption at external and internal solid surfaces of both nonporous and porous structures. A simple use of common isotherms is often misleading because the adsorption of oily components at solid surfaces does not fit the assumptions for which these models were originally derived. This bottleneck then results in problematic calculations of the thermodynamic parameters of sorption.

Author Contributions: Conceptualization, I.K. and M.A.A.-M.; resources, I.K.; data curation, A.T., A.P. and P.S.; writing—original draft preparation, P.S., A.T., A.P. and I.K.; writing—review and editing, I.K., S.A., P.S. and M.A.A.-M.; project administration, I.K.; funding acquisition, I.K., M.A.A.-M. and S.A. All authors have read and agreed to the published version of the manuscript.

Funding: This work was made possible by a grant from the Qatar National Research Fund under its National Priorities Research Program (award number NPRP12S-0311-190299) and by financial support from the ConocoPhillips Global Water Sustainability Center (GWSC). The paper's content is solely the responsibility of the authors and does not necessarily represent the official views of the Qatar National Research Fund or ConocoPhillips. This research was also funded by Qatar University through Qatar University Collaborative Grant QUCGCAM- 20/21-4.

Conflicts of Interest: The authors declare no conflict of interest.

References

1. Pintor, A.M.A.; Vilar, V.J.P.; Botelho, C.M.S.; Boaventura, R.A.R. Oil and grease removal from wastewaters: Sorption treatment as an alternative to state-of-the-art technologies. A critical review. *Chem. Eng. J.* **2016**, *297*, 229–255. [[CrossRef](#)]
2. El-Samak, A.A.; Ponnamma, D.; Hassan, M.K.; Ammar, A.; Adham, S.; Al-Maadeed, M.A.A.; Karim, A. Designing Flexible and Porous Fibrous Membranes for Oil Water Separation—A Review of Recent Developments. *Polym. Rev.* **2020**, *60*, 671–716. [[CrossRef](#)]
3. Ponnamma, D.; Nair, S.S.; Parangusan, H.; Hassan, M.K.; Adham, S.; Karim, A.; Al-Maadeed, M.A.A. White graphene-cobalt oxide hybrid filler reinforced polystyrene nanofibers for selective oil absorption. *Polymers (Basel)* **2020**, *12*, 4. [[CrossRef](#)] [[PubMed](#)]
4. Samanta, A.; Bera, A.; Ojha, K.; Mandal, A. Comparative studies on enhanced oil recovery by alkali-surfactant and polymer flooding. *J. Pet. Explor. Prod. Technol.* **2012**, *2*, 67–74. [[CrossRef](#)]
5. Esmaeilzadeh, P.; Bahramian, A.; Fakhroueian, Z. Adsorption of Anionic, Cationic and Nonionic Surfactants on Carbonate Rock in Presence of ZrO₂ Nanoparticles. *Phys. Procedia* **2011**, *22*, 63–67. [[CrossRef](#)]
6. Gbadamosi, A.O.; Junin, R.; Manan, M.A.; Agi, A.; Yusuff, A.S. An overview of chemical enhanced oil recovery: Recent advances and prospects. *Int. Nano Lett.* **2019**, *9*, 171–202. [[CrossRef](#)]
7. Kamp, J.; Villwock, J.; Kraume, M. Drop coalescence in technical liquid/liquid applications: A review on experimental techniques and modeling approaches. *Rev. Chem. Eng.* **2017**, *33*, 1–47. [[CrossRef](#)]
8. Danov, K.D.; Kralchevsky, P.A.; Ivanov, I.B. *Encyclopedic Handbook of Emulsion Technology*; Marcel Dekker: New York, NY, USA, 2001.
9. Dickinson, E. Emulsion gels: The structuring of soft solids with protein-stabilized oil droplets. *Food Hydrocoll.* **2012**, *28*, 224–241. [[CrossRef](#)]
10. McClements, D.J.; Jafari, S.M. Improving emulsion formation, stability and performance using mixed emulsifiers: A review. *Adv. Colloid Interface Sci.* **2018**, *251*, 55–79. [[CrossRef](#)] [[PubMed](#)]
11. Zhang, T.; Xu, J.; Zhang, Y.; Wang, X.; Lorenzo, J.M.; Zhong, J. Gelatins as emulsifiers for oil-in-water emulsions: Extraction, chemical composition, molecular structure, and molecular modification. *Trends Food Sci. Technol.* **2020**, *106*, 113–131. [[CrossRef](#)]
12. Zembyla, M.; Murray, B.S.; Sarkar, A. Water-in-oil emulsions stabilized by surfactants, biopolymers and/or particles: A review. *Trends Food Sci. Technol.* **2020**, *104*, 49–59. [[CrossRef](#)]
13. Mathavan, G.N.; Viraraghavan, T. Coalescence/filtration of an oil-in-water emulsion in a peat bed. *Water Res.* **1992**, *26*, 91–98. [[CrossRef](#)]
14. Gast, A.P.; Adamson, A.W. *Physical Chemistry of Surfaces*, 6th ed.; Wiley: New York, NY, USA, 1997.
15. Jegatheesan, V.; Vigneswaran, S. Deep bed filtration: Mathematical models and observations. *Crit. Rev. Environ. Sci. Technol.* **2005**, *35*, 515–569. [[CrossRef](#)]
16. El-Naas, M.; Alhaila, M.A. Modelling of adsorption processes. In *Mathematical Modelling*; Brennan, C.R., Ed.; Nova Science Publishers, Inc.: New York, NY, USA, 2011; pp. 579–600.
17. Atkins, P.W.; De Paula, J.; Keeler, J. *Atkins' Physical Chemistry: Quantum Chemistry, Spectroscopy, and Statistical Thermodynamics*, 11th ed.; Oxford University Press: Oxford, UK, 2018.
18. Langmuir, I. The adsorption of gases on plane surfaces of glass, mica and platinum. *J. Am. Chem. Soc.* **1918**, *40*, 1361–1403. [[CrossRef](#)]
19. Albatrni, H.; Qiblawey, H.; Almomani, F.; Adham, S.; Khraisheh, M. Polymeric adsorbents for oil removal from water. *Chemosphere* **2019**, *233*, 809–817. [[CrossRef](#)] [[PubMed](#)]
20. Senthil Kumar, P.; Varjani, S.J.; Suganya, S. Treatment of dye wastewater using an ultrasonic aided nanoparticle stacked activated carbon: Kinetic and isotherm modelling. *Bioresour. Technol.* **2018**, *250*, 716–722. [[CrossRef](#)]
21. Saadi, R.; Saadi, Z.; Fazaali, R.; Fard, N.E. Monolayer and multilayer adsorption isotherm models for sorption from aqueous media. *Korean J. Chem. Eng.* **2015**, *32*, 787–799. [[CrossRef](#)]
22. Akperov, E.O.; Akperov, O.H. The wastage of the cotton stalks (*Gossypium hirsutum* L.) as low-cost adsorbent for removal of the Basic Green 5 dye from aqueous solutions. *Appl. Water Sci.* **2019**, *9*, 209–219. [[CrossRef](#)]
23. Sumanjit; Rani, S.; Mahajan, R.K. Kinetic and Equilibrium Studies of Adsorption of Dye Congo Red from Aqueous Solutions on Bagasse Charcoal and Banana Peels. *J. Surf. Sci. Technol.* **2012**, *28*, 133–147. [[CrossRef](#)]
24. Parker, G.R. Optimum isotherm equation and thermodynamic interpretation for aqueous 1,1,2-trichloroethene adsorption isotherms on three adsorbents. *Adsorption* **1995**, *1*, 113–132. [[CrossRef](#)]
25. Ramakrishna, K.R.; Viraraghavan, T. Dye removal using low cost adsorbents. *Water Sci. Technol.* **1997**, *36*, 189–196. [[CrossRef](#)]
26. Maurya, N.S.; Mittal, A.K. Applicability of equilibrium isotherm models for the biosorptive uptakes in comparison to activated carbon-based adsorption. *J. Environ. Eng.* **2006**, *132*, 1589–1599. [[CrossRef](#)]
27. Edgehill, R.U.; Lu, G.Q. (Max) Adsorption characteristics of carbonized bark for phenol and pentachlorophenol. *J. Chem. Technol. Biotechnol.* **1998**, *71*, 27–34. [[CrossRef](#)]
28. Vázquez, G.; González-Álvarez, J.; García, A.I.; Freire, M.S.; Antorrena, G. Adsorption of phenol on formaldehyde-pretreated Pinus pinaster bark: Equilibrium and kinetics. *Bioresour. Technol.* **2007**, *98*, 1535–1540. [[CrossRef](#)]
29. Miller, C.O.M.; Clump, C.W. A liquid-phase adsorption study of the rate of diffusion of Phenol from aqueous solution into activated Carbon. *AIChE J.* **1970**, *16*, 169–172. [[CrossRef](#)]

30. Ebadi, A.; Soltan Mohammadzadeh, J.S.; Khudiev, A. What is the correct form of BET isotherm for modeling liquid phase adsorption? *Adsorption* **2009**, *15*, 65–73. [[CrossRef](#)]
31. Almeida, E.S.; Carvalho, A.C.B.; de Souza Soares, I.O.; Valadares, L.F.; Mendonça, A.R.V.; Silva, I.J.; Monteiro, S. Elucidating how two different types of bleaching earths widely used in vegetable oils industry remove carotenes from palm oil: Equilibrium, kinetics and thermodynamic parameters. *Food Res. Int.* **2019**, *121*, 785–797. [[CrossRef](#)]
32. Rezvani, H.; Kazemzadeh, Y.; Sharifi, M.; Riazi, M.; Shojaei, S. A new insight into Fe₃O₄-based nanocomposites for adsorption of asphaltene at the oil/water interface: An experimental interfacial study. *J. Pet. Sci. Eng.* **2019**, *177*, 786–797. [[CrossRef](#)]
33. Eskhan, A.; Banat, F. Removal of Oil from Water by Calcium Alginate Hydrogel Modified with Maleic Anhydride. *J. Polym. Environ.* **2018**, *26*, 2901–2916. [[CrossRef](#)]
34. Elgawady, Y.; Ponnamma, D.; Adham, S.; Al-Maas, M.; Ammar, A.; Alamgir, K.; Al-Maadeed, M.A.A.; Hassan, M.K. Mesoporous silica filled smart super oleophilic fibers of triblock copolymer nanocomposites for oil absorption applications. *Emergent Mater.* **2020**, *3*, 1–12. [[CrossRef](#)]
35. Yadav, V.B.; Gadi, R.; Kalra, S. Adsorption of lead on clay-CNT nanocomposite in aqueous media by UV-Vis-spectrophotometer: Kinetics and thermodynamic studies. *Emergent Mater.* **2019**, *2*, 441–451. [[CrossRef](#)]
36. Alberti, G.; Amendola, V.; Pesavento, M.; Biesuz, R. Beyond the synthesis of novel solid phases: Review on modelling of sorption phenomena. *Coord. Chem. Rev.* **2012**, *256*, 28–45. [[CrossRef](#)]
37. Inglezakis, V.J. Solubility-normalized Dubinin-Astakhov adsorption isotherm for ion-exchange systems. *Microporous Mesoporous Mater.* **2007**, *103*, 72–81. [[CrossRef](#)]
38. Furmidge, C.G.L. Studies at phase interfaces. I. The sliding of liquid drops on solid surfaces and a theory for spray retention. *J. Colloid Sci.* **1962**, *17*, 309–324. [[CrossRef](#)]
39. Suteu, D.; Malutan, T. Industrial cellolignin wastes as adsorbent for removal of methylene blue dye from aqueous solutions. *BioResources* **2013**, *8*, 427–446. [[CrossRef](#)]
40. Hamdaoui, O.; Naffrechoux, E. Modeling of adsorption isotherms of phenol and chlorophenols onto granular activated carbon. Part II. Models with more than two parameters. *J. Hazard. Mater.* **2007**, *147*, 401–411. [[CrossRef](#)]
41. Jain, M.; Garg, V.K.; Kadirvelu, K. Chromium(VI) removal from aqueous system using Helianthus annuus (sunflower) stem waste. *J. Hazard. Mater.* **2009**, *162*, 365–372. [[CrossRef](#)]
42. Hu, Q.; Zhang, Z. Application of Dubinin–Radushkevich isotherm model at the solid/solution interface: A theoretical analysis. *J. Mol. Liq.* **2019**, *277*, 646–648. [[CrossRef](#)]
43. Edgar, T.F.; Himmelblau, D.M.; Lasdon, L.S. *Optimization of Chemical Processes*, 2nd ed.; McGraw-Hill: New York, NY, USA, 2001.
44. Hanna, O.T.; Sandall, O.C. *Computational Methods in Chemical Engineering*, Har/Dskt edition; Pearson College Div: Upper Saddle River, NJ, USA, 1995; p. 454.
45. Kumar, K.V. Comparative analysis of linear and non-linear method of estimating the sorption isotherm parameters for malachite green onto activated carbon. *J. Hazard. Mater.* **2006**, *136*, 197–202. [[CrossRef](#)]
46. Lataye, D.H.; Mishra, I.M.; Mall, I.D. Adsorption of 2-picoline onto bagasse fly ash from aqueous solution. *Chem. Eng. J.* **2008**, *138*, 35–46. [[CrossRef](#)]
47. Kumar, K.V.; Porkodi, K.; Rocha, F. Isotherms and thermodynamics by linear and non-linear regression analysis for the sorption of methylene blue onto activated carbon: Comparison of various error functions. *J. Hazard. Mater.* **2008**, *151*, 794–804. [[CrossRef](#)] [[PubMed](#)]
48. Kumar, K.V.; Sivanesan, S. Pseudo second order kinetics and pseudo isotherms for malachite green onto activated carbon: Comparison of linear and non-linear regression methods. *J. Hazard. Mater.* **2006**, *136*, 721–726. [[CrossRef](#)]
49. Tan, I.A.W.; Ahmad, A.L.; Hameed, B.H. Adsorption isotherms, kinetics, thermodynamics and desorption studies of 2,4,6-trichlorophenol on oil palm empty fruit bunch-based activated carbon. *J. Hazard. Mater.* **2009**, *164*, 473–482. [[CrossRef](#)] [[PubMed](#)]
50. Zhao, Y.W.; Shen, B.X.; Sun, H.; Zhan, G.X.; Liu, J.C. Adsorption of dimethyl disulfide on ZSM-5 from methyl tert-butyl ether liquid: A study on equilibrium and kinetics. *Fuel Process. Technol.* **2016**, *145*, 14–19. [[CrossRef](#)]
51. Ceylan, Z.; Mustafaoglu, D.; Malkoc, E. Adsorption of phenol by MMT-CTAB and WPT-CTAB: Equilibrium, kinetic, and thermodynamic study. *Part. Sci. Technol.* **2018**, *36*, 716–726. [[CrossRef](#)]
52. Jung, Y.C.; Bhushan, B. Wetting behavior of water and oil droplets in three-phase interfaces for hydrophobicity/philicity and oleophobicity/philicity. *Langmuir* **2009**, *25*, 14165–14173. [[CrossRef](#)]
53. Salvestrini, S.; Leone, V.; Iovino, P.; Canzano, S.; Capasso, S. Considerations about the correct evaluation of sorption thermodynamic parameters from equilibrium isotherms. *J. Chem. Thermodyn.* **2014**, *68*, 310–316. [[CrossRef](#)]
54. Liu, Y. Some consideration on the Langmuir isotherm equation. *Colloids Surfaces A Physicochem. Eng. Asp.* **2006**, *274*, 34–36. [[CrossRef](#)]
55. Ghosal, P.S.; Gupta, A.K. Determination of thermodynamic parameters from Langmuir isotherm constant-revisited. *J. Mol. Liq.* **2017**, *225*, 137–146. [[CrossRef](#)]
56. Liu, Y. Is the free energy change of adsorption correctly calculated? *J. Chem. Eng. Data* **2009**, *54*, 1981–1985. [[CrossRef](#)]
57. Zhou, X.; Zhou, X. The unit problem in the thermodynamic calculation of adsorption using the Langmuir equation. *Chem. Eng. Commun.* **2014**, *201*, 1459–1467. [[CrossRef](#)]
58. Milonjić, S.K. A consideration of the correct calculation of thermodynamic parameters of adsorption. *J. Serb. Chem. Soc* **2007**, *72*, 1363–1367. [[CrossRef](#)]

59. Azizian, S.; Eris, S.; Wilson, L.D. Re-evaluation of the century-old Langmuir isotherm for modeling adsorption phenomena in solution. *Chem. Phys.* **2018**, *513*, 99–104. [[CrossRef](#)]
60. Lagergren, S. *Zur Theorie der Sogenannten Adsorption Gelöster Stoffe*, Kungliga Svenska Vetenskapsakademiens; Scientific Research Publishing: Handlingar, Sweden, 1898; pp. 1–39.
61. Blanchard, G.; Maunaye, M.; Martin, G. Removal of heavy metals from waters by means of natural zeolites. *Water Res.* **1984**, *18*, 1501–1507. [[CrossRef](#)]
62. Ho, Y.S. Second-order kinetic model for the sorption of cadmium onto tree fern: A comparison of linear and non-linear methods. *Water Res.* **2006**, *40*, 119–125. [[CrossRef](#)]
63. Wang, Z.; Barford, J.P.; Hui, C.W.; McKay, G. Kinetic and equilibrium studies of hydrophilic and hydrophobic rice husk cellulosic fibers used as oil spill sorbents. *Chem. Eng. J.* **2015**, *281*, 961–969. [[CrossRef](#)]
64. Hubbe, M.A.; Azizian, S.; Douven, S. Implications of apparent pseudo-second-order adsorption kinetics onto cellulosic materials: A review. *BioResources* **2019**, *14*, 7582–7626. [[CrossRef](#)]
65. Liu, Y.; Liu, Y.J. Biosorption isotherms, kinetics and thermodynamics. *Sep. Purif. Technol.* **2008**, *61*, 229–242. [[CrossRef](#)]
66. Azizian, S. Kinetic models of sorption: A theoretical analysis. *J. Colloid Interface Sci.* **2004**, *276*, 47–52. [[CrossRef](#)]
67. Ho, Y.S.; McKay, G. Kinetic models for the sorption of dye from aqueous solution by wood. *Process Saf. Environ. Prot.* **1998**, *76*, 183–191. [[CrossRef](#)]
68. Ho, Y.S.; McKay, G. The kinetics of sorption of basic dyes from aqueous solution by sphagnum moss peat. *Can. J. Chem. Eng.* **1998**, *76*, 822–827. [[CrossRef](#)]
69. Ho, Y.S.; McKay, G. A kinetic study of dye sorption by biosorbent waste product pith. *Resour. Conserv. Recycl.* **1999**, *25*, 171–193. [[CrossRef](#)]
70. Ho, Y.S.; McKay, G. Sorption of dye from aqueous solution by peat. *Chem. Eng. J.* **1998**, *70*, 115–124. [[CrossRef](#)]
71. Canzano, S.; Iovino, P.; Leone, V.; Salvestrini, S.; Capasso, S. Use and misuse of sorption kinetic data: A common mistake that should be avoided. *Adsorpt. Sci. Technol.* **2012**, *30*, 217–225. [[CrossRef](#)]
72. Douven, S.; Paez, C.A.; Gommès, C.J. The range of validity of sorption kinetic models. *J. Colloid Interface Sci.* **2015**, *448*, 437–450. [[CrossRef](#)]
73. Crank, J. *The Mathematics of Diffusion*, 2nd ed.; Oxford University Press: London, UK, 1975; pp. 69–88.
74. Weber, W.J.; Morris, J.C. Kinetics of Adsorption on Carbon from Solution. *J. Sanit. Engineer. Div.* **1963**, *89*, 31–60. [[CrossRef](#)]
75. Réguer, A.; Sochard, S.; Hort, C.; Platel, V. Measurement and modelling of adsorption equilibrium, adsorption kinetics and breakthrough curve of toluene at very low concentrations on to activated carbon. *Environ. Technol.* **2011**, *32*, 757–766. [[CrossRef](#)]
76. Thomas, H.C. Heterogeneous Ion Exchange in a Flowing System. *J. Am. Chem. Soc.* **1944**, *66*, 1664–1666. [[CrossRef](#)]
77. Juang, R.S.; Kao, H.C.; Chen, W. Column removal of Ni(II) from synthetic electroplating waste water using a strong-acid resin. *Sep. Purif. Technol.* **2006**, *49*, 36–42. [[CrossRef](#)]
78. Janson, A.; Minier-Matar, J.; Al-Shamari, E.; Hussain, A.; Sharma, R.; Rowley, D.; Adham, S. Evaluation of new ion exchange resins for hardness removal from boiler feedwater. *Emergent Mater.* **2018**, *1*, 77–87. [[CrossRef](#)]
79. Pintor, A.M.A.; Martins, A.G.; Souza, R.S.; Vilar, V.J.P.; Botelho, C.M.S.; Boaventura, R.A.R. Treatment of vegetable oil refinery wastewater by sorption of oil and grease onto regranulated cork—A study in batch and continuous mode. *Chem. Eng. J.* **2015**, *268*, 92–101. [[CrossRef](#)]
80. Bohart, G.S.; Adams, E.Q. Some aspects of the behavior of charcoal with respect to chlorine. *J. Am. Chem. Soc.* **1920**, *42*, 523–544. [[CrossRef](#)]
81. Hutchins, R.A. New method simplifies design of activated carbon systems. *Chem. Engineer.* **1973**, *80*, 133–135.
82. Elmobarak, W.F.; Almomani, F. Application of Fe₃O₄ magnetite nanoparticles grafted in silica (SiO₂) for oil recovery from oil in water emulsions. *Chemosphere* **2021**, *265*, 129054. [[CrossRef](#)] [[PubMed](#)]
83. Ewis, D.; Benamor, A.; Ba-Abbad, M.M.; Nasser, M.; El-Naas, M.; Qiblawey, H. Removal of Oil Content from Oil-Water Emulsions Using Iron Oxide/Bentonite Nano Adsorbents. *J. Water Process Eng.* **2020**, *38*, 2214–7144. [[CrossRef](#)]
84. Diraki, A.; Mackey, H.; McKay, G.; Abdala, A.A. Removal of oil from oil–water emulsions using thermally reduced graphene and graphene nanoplatelets. *Chem. Eng. Res. Des.* **2018**, *137*, 47–59. [[CrossRef](#)]
85. Lin, K.-Y.A.; Chen, Y.-C.; Phattarapattamawong, S. Efficient demulsification of oil-in-water emulsions using a zeolitic imidazolate framework: Adsorptive removal of oil droplets from water. *J. Colloid Interface Sci.* **2016**, *478*, 97–106. [[CrossRef](#)]
86. Wang, D.; McLaughlin, E.; Pfeffer, R.; Lin, Y.S. Adsorption of oils from pure liquid and oil–water emulsion on hydrophobic silica aerogels. *Sep. Purif. Technol.* **2012**, *99*, 28–35. [[CrossRef](#)]
87. Elanchezhian, S.S.; Prabhu, S.M.; Meenakshi, S. Effective adsorption of oil droplets from oil-in-water emulsion using metal ions encapsulated biopolymers: Role of metal ions and their mechanism in oil removal. *Int. J. Biol. Macromol.* **2018**, *112*, 294–305. [[CrossRef](#)]
88. Okiel, K.; El-Sayed, M.; El-Kady, M.Y. Treatment of oil–water emulsions by adsorption onto activated carbon, bentonite and deposited carbon. *Egypt. J. Pet.* **2011**, *20*, 9–15. [[CrossRef](#)]
89. Wu, M.; Zhai, M.; Li, X. Adsorptive removal of oil drops from ASP flooding-produced water by polyether polysiloxane-grafted ZIF-8. *Powder Technol.* **2021**, *378*, 76–84. [[CrossRef](#)]

90. Sharma, M.; Joshi, M.; Nigam, S.; Avasthi, D.K.; Adelung, R.; Srivastava, S.K.; Mishra, Y.K. Efficient oil removal from wastewater based on polymer coated superhydrophobic tetrapodal magnetic nanocomposite adsorbent. *Appl. Mater. Today* **2019**, *17*, 130–141. [[CrossRef](#)]
91. Venkatesh, K.; Arthanareeswaran, G.; Bose, A.C.; Kumar, P.S. Hydrophilic hierarchical carbon with TiO₂ nanofiber membrane for high separation efficiency of dye and oil-water emulsion. *Sep. Purif. Technol.* **2020**, *241*, 116709. [[CrossRef](#)]
92. Knapik, E.; Stopa, J. Fibrous deep-bed filtration for oil/water separation using sunflower pith as filter media. *Ecol. Eng.* **2018**, *121*, 44–52. [[CrossRef](#)]
93. El-Maghrabi, H.H.; Hosny, R.; Ramzi, M.; Zayed, M.A.; Fathy, M. Preparation and Characterization of Novel Magnetic ZnFe₂O₄-Hydroxyapatite Core-Shell Nanocomposite and Its Use as Fixed Bed Column System for Removal of Oil Residue in Oily Wastewater Samples. *Egypt. J. Pet.* **2019**, *28*, 137–144. [[CrossRef](#)]
94. Akpomie, K.G.; Conradie, J. Ultrasonic aided sorption of oil from oil-in-water emulsion onto oleophilic natural organic-silver nanocomposite. *Chem. Eng. Res. Des.* **2021**, *165*, 12–24. [[CrossRef](#)]
95. Elanchezhian, S.S.; Meenakshi, S. Synthesis and characterization of chitosan/Mg-Al layered double hydroxide composite for the removal of oil particles from oil-in-water emulsion. *Int. J. Biol. Macromol.* **2017**, *104*, 1586–1595. [[CrossRef](#)]
96. Ben-Avraham, D. Van der Waals Forces: A Handbook for Biologists, Chemists, Engineers, and Physicists. *J. Stat. Phys.* **2006**, *123*, 709–710. [[CrossRef](#)]
97. An essay on the cohesion of fluids. *Abstr. Pap. Print. Philos. Trans. R. Soc. London* **1832**, *1*, 171–172. [[CrossRef](#)]
98. Whyman, G.; Bormashenko, E.; Stein, T. The rigorous derivation of Young, Cassie-Baxter and Wenzel equations and the analysis of the contact angle hysteresis phenomenon. *Chem. Phys. Lett.* **2008**, *450*, 355–359. [[CrossRef](#)]
99. Shafrin, E.G.; Zisman, W.A. Constitutive relations in the wetting of low energy surfaces and the theory of the retraction method of preparing monolayers. *J. Phys. Chem.* **1960**, *64*, 519–524. [[CrossRef](#)]
100. Good, R.J.; van Oss, C.J. The Modern Theory of Contact Angles and the Hydrogen Bond Components of Surface Energies BT. In *Modern Approaches to Wettability: Theory and Applications*; Schrader, M.E., Loeb, G.I., Eds.; Springer Science + Business media: New York, NY, USA, 1992; pp. 1–27.
101. Cassie, A.B.D.; Baxter, S. Wettability of porous surfaces. *Trans. Faraday Soc.* **1944**, *40*, 546–551. [[CrossRef](#)]
102. Marmur, A. Thermodynamic aspects of contact angle hysteresis. *Adv. Colloid Interface Sci.* **1994**, *50*, 121–141. [[CrossRef](#)]
103. Gao, L.; McCarthy, T.J. Contact angle hysteresis explained. *Langmuir* **2006**, *22*, 6234–6237. [[CrossRef](#)]
104. Ge, J.; Zhao, H.Y.; Zhu, H.W.; Huang, J.; Shi, L.A.; Yu, S.H. Advanced Sorbents for Oil-Spill Cleanup: Recent Advances and Future Perspectives. *Adv. Mater.* **2016**, *28*, 10459–10490. [[CrossRef](#)]
105. Chen, C.; Weng, D.; Mahmood, A.; Chen, S.; Wang, J. Separation Mechanism and Construction of Surfaces with Special Wettability for Oil/Water Separation. *ACS Appl. Mater. Interfaces* **2019**, *11*, 11006–11027. [[CrossRef](#)]
106. Hubbe, M.A.; Gardner, D.J.; Shen, W. Contact angles and wettability of cellulosic surfaces: A review of proposed mechanisms and test strategies. *BioResources* **2015**, *10*, 8657–8749. [[CrossRef](#)]
107. Yong, J.; Chen, F.; Yang, Q.; Huo, J.; Hou, X. Superoleophobic surfaces. *Chem. Soc. Rev.* **2017**, *46*, 4168–4217. [[CrossRef](#)] [[PubMed](#)]
108. Xue, Z.; Liu, M.; Jiang, L. Recent developments in polymeric superoleophobic surfaces. *J. Polym. Sci. Part B Polym. Phys.* **2012**, *50*, 1209–1224. [[CrossRef](#)]
109. Liu, M.; Wang, S.; Wei, Z.; Song, Y.; Jiang, L. Superoleophobic Surfaces: Bioinspired Design of a Superoleophobic and Low Adhesive Water/Solid Interface (Adv. Mater. 6/2009). *Adv. Mater.* **2009**, *21*, 665–669. [[CrossRef](#)]
110. Järn, M.; Granqvist, B.; Lindfors, J.; Kallio, T.; Rosenholm, J.B. A critical evaluation of the binary and ternary solid-oil-water and solid-water-oil interaction. *Adv. Colloid Interface Sci.* **2006**, *123–126*, 137–149. [[CrossRef](#)] [[PubMed](#)]
111. Hubbe, M.A.; Rojas, O.J.; Fingas, M.; Gupta, B.S. Cellulosic Substrates for Removal of Pollutants from Aqueous Systems: A Review. 3.Spilled Oil and Emulsified Organic Liquids. *BioResources* **2013**, *8*, 3038. [[CrossRef](#)]
112. Parangusan, H.; Ponnamma, D.; Hassan, M.K.; Adham, S.; Al-Maadeed, M.A.A. Designing carbon nanotube-based oil absorbing membranes from gamma irradiated and electrospun polystyrene nanocomposites. *Materials (Basel)* **2019**, *12*, 709. [[CrossRef](#)]
113. Fahim, M.A.; Othman, F.M. Coalescence of secondary dispersions in composite packed beds. *J. Dispers. Sci. Technol.* **1987**, *8*, 507–523. [[CrossRef](#)]
114. Hadjiev, D.; Aurelle, Y.; Assenov, A. New separator for removal of organic liquids in water. *Environ. Technol. (UK)* **1992**, *13*, 267–274. [[CrossRef](#)]
115. Kang, W.; Li, M.; Yang, H.; Kang, X.; Wang, F.; Jiang, H.; Zhang, M.; Zhu, T.; Sarsenbekuly, B. Coalescence behavior of aqueous drops in water-in-oil emulsions under high-frequency pulsed AC fields. *J. Ind. Eng. Chem.* **2021**, *93*, 415–422. [[CrossRef](#)]
116. Head, B.A. Method of Filtering Oil from Oil-and-Water Emulsions. U.S. Patent 4309289A, 5 January 1982.
117. Šećerov Sokolović, R.M.; Govedarica, D.D.; Sokolović, D.S. Separation of oil-in-water emulsion using two coalescers of different geometry. *J. Hazard. Mater.* **2010**, *175*, 1001–1006. [[CrossRef](#)]
118. Rawlins, C.H. Experimental Study on Oil and Solids Removal in Nutshell Filters for Produced Water Treatment. In Proceedings of the SPE Western Regional Meeting, Garden Grove, CA, USA, 22–27 April 2018.
119. Agarwal, S.; Von Arnim, V.; Stegmaier, T.; Planck, H.; Agarwal, A. Role of surface wettability and roughness in emulsion separation. *Sep. Purif. Technol.* **2013**, *107*, 19–25. [[CrossRef](#)]
120. Agarwal, S.; Von Arnim, V.; Stegmaier, T.; Planck, H.; Agarwal, A. Effect of fibrous coalescer geometry and operating conditions on emulsion separation. *Ind. Eng. Chem. Res.* **2013**, *52*, 13164–13170. [[CrossRef](#)]

121. Mino, Y.; Kagawa, Y.; Matsuyama, H.; Ishigami, T. Permeation of oil-in-water emulsions through coalescing filter: Two-dimensional simulation based on phase-field model. *AIChE J.* **2016**, *62*, 2525–2532. [[CrossRef](#)]
122. Bansal, S.; von Arnim, V.; Stegmaier, T.; Planck, H. Effect of fibrous filter properties on the oil-in-water-emulsion separation and filtration performance. *J. Hazard. Mater.* **2011**, *190*, 45–50. [[CrossRef](#)] [[PubMed](#)]
123. Fredrick, E.; Walstra, P.; Dewettinck, K. Factors governing partial coalescence in oil-in-water emulsions. *Adv. Colloid Interface Sci.* **2010**, *153*, 30–42. [[CrossRef](#)] [[PubMed](#)]
124. Soma, J.; Papadopoulos, K.D. Deposition of oil-in-water emulsions in sand beds in the presence of cetyltrimethylammonium bromide. *Environ. Sci. Technol.* **1997**, *31*, 1040–1045. [[CrossRef](#)]
125. Shukla, A.; Zhang, Y.H.; Dubey, P.; Margrave, J.L.; Shukla, S.S. The role of sawdust in the removal of unwanted materials from water. *J. Hazard. Mater.* **2002**, *95*, 137–152. [[CrossRef](#)]